Author version: *Clim. Dyn., vol.38; 2012; 1521-1543*

TropFlux: Air-Sea Fluxes for the Global Tropical Oceans – Description and evaluation against observations

B. Praveen Kumar[1], J. Vialard[1 2], M. Lengaigne[1 2], V.S.N. Murty[3], M.J. McPhaden[4]

1. National Institute of Oceanography, Council of Scientific and Industrial Research (CSIR), Goa, India.

2. Laboratoire d'Océanographie Expérimentation et Approches Numériques, CNRS, UPMC, IRD, Paris, France.

3. National Institute of Oceanography Regional Centre, Council of Scientific and Industrial Research (CSIR), Visakhapatnam, India.

4. NOAA/Pacific Marine Research Laboratory, Seattle, Washington, USA.

Corresponding author: B Praveen Kumar (bpraveen@nio.org)

Abstract

The purpose of this paper is to evaluate several timely, daily air-sea flux products (NCEP, NCEP2, ERA-Interim and OAFlux/ISCCP) against observations and to present a newly developed air-sea flux product (TropFlux). Evaluation of basic variables used for bulk turbulent flux estimates (sea surface temperature, air temperature and humidity at 2m height and wind at 10m height) to observations from the global tropical moored array reveals that the recently released ERA-Interim data generally captures best the temporal variability (with correlations above 0.85 with mooring data) despite strong systematic biases in surface temperature and humidity, and underestimation of variance. Shortwave radiations from various re-analyses are generally inferior to those from the ISCCP project. Longwave radiations from all sources have low correlations with mooring observations (0.3 to 0.6), but with ISCCP and ERA-Interim performing best (give the correlation value here).

We use mooring data to correct the systematic bias and amplitude of ERA-Interim basic meteorological variables, used as input to the COARE v3.0 algorithm. Wind speed is also corrected to take mesoscale wind gustiness into account, based on the linear fit between climatological sea surface temperature and gustiness values estimated from mooring data. We use the bias and amplitude corrected ERA-Interim surface net longwave radiation. Surface net shortwave radiation (SWR) is based on ISCCP, with a systematic bias and variability amplitude correction. The timeliness of the TropFlux product is limited by the availability of ISCCP SWR products, so we extend the time series by using a "near real-time" SWR estimated from outgoing longwave radiation (OLR) non-seasonal anomalies. The near real-time mode shortwave data performs well over convective regions but underestimates variability over the cold tongues of the Atlantic and Pacific. This timely estimate of SWR however performs better than the commonly used re-analysis SWR products.

All products agree well in reproducing intraseasonal surface net heat fluxes fluctuations associated with the Madden-Julian Oscillation in the Indian Ocean, and interannual heat flux variations associated with El Niño in the eastern Pacific. They do however exhibit marked differences in mean values and seasonal cycle. Comparison to global tropical moored array, I-COADS and fully independent flux data suggests that TropFlux and OAFlux net heat fluxes are superior to the three re-analyses. TropFlux hence provides a useful option for studying flux variability associated with ocean-atmosphere interactions, oceanic heat budgets and climate fluctuations in the tropics.

1. Introduction

The tropics are an essential part of the Earth's climate. In addition of being home to the Indo-Pacific warm-pool, the largest area of deep atmospheric convection on earth, they are also source of very significant variability at intraseasonal to interannual timescales. Interannual variability develops as the result of air-sea interactions in all three oceans. El Niño–Southern Oscillation (ENSO) affects weather patterns at a global scale (e.g. McPhaden et al. 2006). Interannual variability with clear climatic consequences in the Indian Ocean has also been identified more recently in the tropical Indian Ocean (the Indian Ocean Dipole or IOD, e.g. Saji et al. 1999; Webster et al. 1999). In the Atlantic Ocean, significant ocean-atmosphere variability is developed by fluctuations in the Atlantic Meridional Mode or AMM (is it different from North Atlantic Oscillation (NAO)) (Xie and Carton. 2004; Chiang and Vimont. 2004). At intraseasonal timescale, the Madden Julian-Oscillation (MJO, Madden and Julian. 1972) modulates the Asian, African and Australian monsoons, tropical cyclone activity and even the weather regimes over the North Atlantic (Cassou. 2008). A better understanding of these phenomena are required to improve predictability at intraseasonal to interannual timescales.

Air-sea coupling plays a prominent role in the whole range of phenomena described above. Air-sea interactions are vital for the development of ENSO and the IOD through the Bjerknes feedback (Bjerknes. 1966), which involves reinforcing tendencies in surface winds and sea surface temperature (SST). In both cases, a proper knowledge of air-sea fluxes is needed to understand the processes of interannual variability better. Air-sea fluxes act as a strong negative feedback to ENSO in the eastern Pacific (Wang and McPhaden, 2000; Vialard et al. 2001), and can contribute either positively or negatively to IOD growth depending on the season and location (Hendon 2003; Murtugudde et al. 2000). Remotely forced surface heat flux variations are essential to explain the overall Indian Ocean warming during El Niño (Klein et al. 1999). Latent heat flux variations are the key mechanism for explaining the wind-evaporation-SST feedback involved in the AMM development (Xie and Philander. 1994; Vimont and Kossin. 2007).

At intraseasonal timescales, the MJO is largely due to the result of atmospheric internal dynamics. While air–sea coupling is not necessary for the MJO to develop, it generally strengthens and organizes simulated MJO signals (Zhang et al. 2006). The MJO is associated with clear SST intraseasonal variability, in particular in the Indian Ocean and maritime continent regions (Duvel and Vialard. 2007). Heat flux variability is a major contributor to this SST variability in the Indian Ocean (Vialard et al. 2008; Jayakumar et al. 2011; Vialard et al. 2011). In addition to explaining the SST signature of the MJO, Sobel et al. (2008) argue that heat fluxes from ocean to

atmosphere play a fundamental role in driving the intraseasonal oscillation itself. Accurate determination of intraseasonal to interannual air-sea fluxes variability is thus a prerequisite for better understanding the tropical mean climate and variability.

Earliest attempts for estimating the air-sea fluxes can be traced back to the pioneering works of Budkyo (1963), Bunker (1976), Bunker and Worthington (1976) and Perry and Walker (1977). These efforts to estimate air-sea fluxes using atmospheric and oceanic variables collected during ship cruises, together with empirical formula were generally restricted to some specific oceanic basins. The Comprehensive Ocean-Atmosphere Dataset (COADS: Elms et al. 1993, Woodruff et al. 1993) is an attempt to provide a global database of relevant input parameters for estimating air-sea fluxes. National Oceanography Centre Southampton – NOCS (previously SOC flux) Flux data (Josey et al. 1999; Berry and Kent. 2009) is based on the COADS dataset and the data gaps are filled with advanced interpolation methods. But spatio-temporal interpolation in the vast gaps between ship regular routes is a major source of uncertainty in these products, and only allows low-temporal resolution (monthly estimates), which does not suit the study of intraseasonal variability.

Atmospheric re-analyses partly overcome this drawback, by using atmospheric general circulation models to carry information forward in time, and then elaborate interpolation methods to combine them with available observations. The NCEP/NCAR (Kalnay et al. 1996), NCEP2 (Kanamitsu et al. 2002) and ERA-40 (Uppala et al. 2005) re-analyses hence provide more than 40 years of daily net heat flux products, but do however suffer from model error. Improvement of satellite technology led to the development of satellite observations based flux products like J-OFURO (Kubota et al. 2002) and HOAPS (Schulz and Bakan. 1998). The major drawback of such data products is the limited length of the satellite measurements, since most accurate and precise measurements are available only from 2000 onwards. Another challenging problem in satellite measurements is the accurate estimation of air temperature and specific humidity at a particular height above the sea surface (Yu and Weller. 2007). The objective analysis method used in OAFlux (Yu et al. 2007; Yu and Weller. 2007) in principle combines optimally satellite measurements and model reanalysis. Hybrid turbulent heat flux products based on satellite measurements and numerical weather prediction model outputs have also been developed (e.g. Jiang et al. 2005).

In all these cases, evaluation of the heat flux products to estimates obtained more directly from *in situ* measurements is necessary. The Global Tropical Moored Buoy Array is the combination of the TAO/TRITON in the Pacific (McPhaden et al. 1998), PIRATA in the Atlantic (Bourles et al. 2008) and RAMA in the Indian Ocean (McPhaden et al. 2009). These arrays provide an unprecedented opportunity to estimate surface heat fluxes in the three tropical oceans. The moorings in these arrays provide near-real time *in situ* measurements of essential parameters to estimate the

surface net heat fluxes: near-surface wind, air temperature, humidity, SST as well as downward shortwave and longwave fluxes. These can be used in combination with the COARE v3.0 algorithm (Fairall et al. 2003) to provide reliable estimates of the surface heat fluxes (Cronin et al. 2006).

This study takes advantage of this mooring database to provide an evaluation of air-sea fluxes and flux related parameters from various sources in the tropics. We will restrict our analysis to products that resolve intraseasonal variability (daily resolution). We will also focus on near-realtime or regularly updated products in order to be able to benefit from lengthening time-series in the Atlantic and Indian Oceans where PIRATA and RAMA were setup much more recently than TAO/TRITON. Table 1 shows that 4 products meet these constraints: OAFlux/ISCCP, NCEP, NCEP2 and ERA-Interim (hereafter ERA-I). We will show in this paper that ERA-I near-surface parameters generally provide better performance in terms of phasing with observations, despite systematic biases. We hence develop a simple correction method that allows estimation of a new net heat flux product in the tropics (TropFlux) from ERA-I corrected parameters. Independent flux estimates will also be used to validate our correction approach.

This paper is constructed as follows. Section 2 presents the various datasets used in this study. In section 3, the input variables necessary for turbulent flux computations are evaluated against *in situ* data from the global tropical moored buoy array. We then explain in section 4 how we build on existing datasets (mainly on ERA-I, ISCCP and NOAA OLR data) to construct a new, timely product of daily heat fluxes for the tropics: TropFlux. Since tropical moored array data was used to construct the TropFlux product, it cannot be used for a real validation of this product. In section 5, we provide validation of the various flux products in this study against independent data. We also illustrate how these products capture some important intraseasonal and interannual variations. Section 6 provides a summary the results of this paper and a discussion.

2. Datasets and methods

In this section we first briefly review the basics of obtaining air-sea fluxes using a bulk parameter approach. We then describe the various surface meteorological and air-sea flux products that are evaluated in this study. We finally describe the *in-situ* data from the global tropical moored buoy array used for developing *ad-hoc* corrections and independent data from five mooring experiments in geographically distinct regions of the tropical oceans, which are used for independent validation.

a. Bulk estimation of fluxes

The net air-sea flux at the sea surface is given by the sum of net radiative fluxes (longwave and shortwave radiations, hereafter LWR_{net} and SWR_{net} respectively) and turbulent fluxes (latent and sensible heat fluxes; hereafter LHF and SHF respectively). A commonly used approach to compute these air-sea fluxes is to use bulk formulae, which relate the various flux components to meteorological parameters such as wind, air temperature, specific humidity and sea surface temperature (Fairall et al. 1996; Curry et al. 2004):

$$LHF = \rho L_e C_e U Q_s - Q_a) \quad (1)$$

$$SHF = \rho C_p C_h U (SST-T_a) \quad (2)$$

$$LWR_{net}= \varepsilon\sigma T_s^4-LWR_{down} \quad (3)$$

$$SWR_{net}= (1-a)SWR_{down} \quad (4)$$

$$NET=SWR_{net}-(LWR_{net}+LHF+SHF) \quad (5)$$

where, ρ is the density of air, L_e is the latent heat of evaporation, C_e and C_h are the turbulent exchange coefficients for latent and sensible fluxes respectively, C_p is the specific heat capacity of air at constant pressure, U is the wind speed relative to sea surface, Q_s and Q_a are saturation specific humidity at sea surface temperature and near-surface atmospheric specific humidity respectively and SST and T_a are sea surface and air temperature respectively, a is the surface albedo (set to 0.055 in this study), surface emissivity ε is 0.97, and σ is the Stefan Boltzman constant. With the convention above (downward fluxes for shortwave and upward fluxes for the other components), all flux components are almost always positive.

A variety of bulk flux algorithms differing in their parameterization of exchange coefficients, salinity effect on sea surface humidity, and treatment of free convective conditions and surface layer gustiness are available (e.g. Smith. 1988; Clayson et al. 1996; Zeng et al. 1998; Bourassa et al. 1999; Fairall et al. 2003). Intercomparison of turbulent flux algorithms (Brunke et al. 2002, 2003) shows that the 3rd version of the Coupled Ocean-Atmosphere Response Experiment bulk flux algorithm (COARE v3.0, Fairall et al. 2003) displays the lowest bias compared to algorithms used to produce the HOAPS (Schulz and Bakan. 1998; Grassl et al. 2000; Andersson et al. 2007), GSSTF-2 (Chou et al. 2004) and J-OFURO (Kubota et al. 2002) flux data sets. Hence, we use COARE v3.0 algorithm in the present study.

The COARE algorithm was initially developed for the COARE research community to estimate air-sea fluxes under the strong convective conditions of the western Pacific warm pool (Fairall et al. 1996) and later modified for colder waters and higher wind speeds conditions, i.e. mid-

latitude conditions (Bradley et al. 2000; Fairall et al. 2003). Significant improvements have been made on COARE v3.0 bulk flux algorithm from its previous versions. Wind speed validity is now extended to 0-20m/s; improvements have also been made on the stability functions.

In this paper, we use daily averages of basic meteorological variables (U, T_a, Q_a, SST) as inputs to the COARE algorithm. The COARE algorithm is tuned for use with hourly averaged data (Fairall et al. 2003), and cool skin and warm layer calculation should be switched off for use with daily data (Cronin et al 2006). Fairall et al (1996) and Cronin et al (2006) estimated that ignoring the cool skin effect would produce an error of around 10 Wm^{-2} in the latent heat flux. A gustiness parameterization is also included to account for high frequency wind variations as recommended by Cronin et al. (2006). We will describe the gustiness correction approach in more detail in section 4.

There are several studies describing the estimate of longwave radiation using empirical formulae (e.g. Clark et al. 1974, Bignami et al. 1995, Josey et al. 1997, Josey et al. 2003). Josey et al (1997) evaluated the atmospheric component of several longwave formulae using research cruise data and found that Clark's empirical formulae works best. Josey et al (1997) therefore used Clark's method as did several other studies (e.g. Cronin et al. 2006; Foltz and McPhaden. 2005; Foltz et al. 2010). Josey et al (2003) provided an improved longwave radiation formula for mid-latitude but did not test it in the tropical regions. We will hence evaluate Clark et al. (1974) empirical formula against the other products in this paper. In Clark et al. (1974), the net longwave radiation is estimated from:

$$LWRNet = \varepsilon\sigma SST^4 (0.39 - 0.05e_a^{1/2})(1 - 0.51C^2) + 4\varepsilon\sigma T_s^3 (SST - T_a) \quad (6),$$

where ε is the emissivity, σ is the Stephan-Boltzmann constant, SST and T_a are sea surface and air temperature at 2m respectively e_a is the surface vapor pressure and C is the cloud cover index. Following Foltz and McPhaden (2005) this cloud cover can be estimated from SWR_{down} using an inversion of Reed's (1997) formula:

$$C = 1.61(1 - SWR / SWR_{cs} + 0.0019n) \quad (7),$$

where SWR is the daily-averaged surface shortwave radiation, SWR_{cs} is the clear-sky radiation, and n is the noon time solar altitude.

b. Surface meteorological and air-sea flux datasets

In this section, we describe the source of various data products that we use in this paper: satellite-derived U and SST; all four heat flux components and near surface meteorological parameters (SST, T_a, Q_a and U) from OAFlux (Yu et al. 2007) product, NCEP (Kalnay et al. 1996),

NCEP2 (Kanamitsu et al. 2002) and ERA-I (Dee and Uppala. 2009) re-analyses products. All of the products described below were regridded on the 1° x 1° OAFlux grid.

Three satellite products are used in this paper. For SST, we use optimally interpolated data from the TRMM Microwave Imager (TMI) instrument produced by Remote Sensing Systems (http://www.remss.com/). One important feature of this microwave retrieval is that SST can be measured through clouds (Kummerow et al. 1998) and captures very satisfactorily intraseasonal SST variations in highly convective regions (e.g. Duvel and Vialard 2007). TMI SST is originally available at 0.25°, daily resolution from December 1997 to the present time. For winds, we use gridded estimates of 10-m winds from the QuikSCAT scatterometer produced at Centre ERS d'Archivage et de Traitement (CERSAT, Bentamy et al. 2003). QuickSCAT uses rain flags to identify and mask rainy pixels in its data and hence will be more accurate over convective regions (Weissman et al. 2002). Wind data from QuikSCAT are available at 0.25°, from July 1999 to November 2009. We also use Outgoing Longwave Radiation (OLR) data to provide a near-realtime extension of the surface shortwave radiation estimate. OLR data is obtained from NOAA, with gaps filled with temporal and spatial interpolation (Liebmann and Smith. 1996).

We use near surface meteorological variables and surface fluxes from NCEP, NCEP2, and the recently released ERA-interim (ERA-I) re-analyses. We did not include ERA40 in our analysis since it is only available until 2002, and most moorings were deployed after this date in the Atlantic and Indian Oceans. The NCEP/NCAR Reanalysis 1 (NCEP) is using a state-of-the-art analysis/forecast system to perform data assimilation using past data from 1948 to the present (Kalney et al. 1996). Fluxes and related meteorological variables are available at NCEP on global grids at 1.90° x 1.87° resolutions. NCEP-DOE Reanalysis 2 (NCEP2) is an improved version of the NCEP Reanalysis that fixed errors and updated parameterizations of physical processes (Kanamitsu et al. 2002). NCEP2 differs from NCEP reanalysis mainly in shortwave radiation scheme, cloud and soil moisture parameterizations, improved desert albedo, introduction of new ozone climatology etc. Daily data from NCEP 2 are available globally from 1979 to 2009 on 1.90° x 1.87° grids. Both NCEP and NCEP2 input variables are obtained from 6-hourly forecasts. ERA-I is the latest ECMWF global atmospheric reanalysis for the period 1989 to present with major improvements over its past re-analysis product ERA-40 (Dee and Uppala. 2009). The major differences between the earlier release ERA-40 and the latest ERA-I are the use of a 4D-Var approach, a better formulation of background error constraints, a new humidity analysis, improved model physics, improved data quality control methods, and improvements in bias handling. Global data from ERA-I are available at 0.75° x 0.75° spatial resolution. The ERA-I input variables (wind, surface and air temperature and humidity) were computed from the average of 4 times daily analyzed fields, while the fluxes were

obtained from the 0 to 24h forecast average. NCEP is updated in near real time, whereas NCEP2 is updated on a yearly basis and ERA-I data production lags 3-4 months behind real time (Table 1).

OAFlux surface fluxes are obtained from blending of various satellite retrievals and re-analysis products (Yu et al. 2007). Consensus estimates of surface meteorological variables from these sources are obtained through a variational method. Turbulent air-sea fluxes are then estimated through application of COARE v3.0 algorithm (Fairall et al. 2003). The OAFlux product was initially developed for the Atlantic Ocean over the 1988-1999 period (Yu et al. 2004a,b, 2006) and later extended to the Indian Ocean (Yu et al. 2007) and global ocean basins over the 1981-2007 period (Yu and Weller. 2007). OAFlux does not provide its own estimates of radiative fluxes, but rather uses net surface shortwave and longwave daily values from the International Satellite Cloud Climatology (ISCCP) project (Zhang et al. 2004).

The ISCCP project uses an advanced radiative transfer model to produce radiative fluxes, at a 3-hourly, 2.5° x 2.5° resolution, based on various (largely satellite) input datasets providing the needed properties of clouds, atmosphere and surface. OAFlux project provides surface net radiative fluxes from ISCCP after interpolating them into the daily, 1° x 1° OAFlux grid. OAFlux is a timely product (it is updated twice a year, and available until July 2010 at the time of writing). The availability of net heat fluxes is however limited by the availability of ISCCP radiative fluxes. ISCCP is updated once in a few years, and available until 2007 at the time of writing. Providing an alternative to complement ISCCP data until near-realtime is an issue that we will explore in this paper.

c. Evaluation dataset: the tropical moored array data

The Global Tropical Moored Buoy Array (hereafter TPR, for TAO/TRITON-PIRATA-RAMA) is a multi-national effort to provide real time meteorological and oceanographic data for the research community and operational applications. It has three components, namely TAO/TRITON in the Pacific (McPhaden et al. 1998), PIRATA in the Atlantic (Bourles et al. 2008) and RAMA in the Indian Ocean (McPhaden et al. 2009). The three arrays have been designed in order to provide high-resolution surface (and subsurface) time-series in climatically relevant regions. The TAO array has been completed for more than 10 years and provides the longest record (Fig. 1), while PIRATA has only recently been completed and RAMA was only ~55% complete in mid 2010 (21 out of 38 planned moorings).

We have used daily average data in this paper (higher temporal resolution data is not available for the full length of the record, and its use would shorten drastically some time series in the Indian Ocean). TPR data undergo extensive quality control analysis to ensure that they meet stringent

accuracy standards (Freitag et al. 1999, 2001; Medavaya et al. 2002; Payne et al. 2002; Lake et al. 2003). We use only the highest quality observations from these moorings for evaluation (flags 1-2: highest quality or default quality).

Air temperature and humidity (hereafter T_a and Q_a) are measured at about 3 m height on the moorings. The TPR humidity data is provided as relative humidity and converted into specific humidity (Bolton. 1980). We compare TPR data directly with other products, which provide air-temperature and humidity at 2m above the surface. SST is measured 1m below the surface.

Wind speed (hereafter w_a) is measured at about 4m-height on the moorings. We convert this to 10m-height wind using a logarithmic profile method (Mears et al. 2001). Mears et al. (2001) and Parekh et al. (2007) compared this simple logarithmic approach with a more sophisticated approach, which requires air temperature, atmospheric pressure and relative humidity and concluded that the differences between the two wind transforming schemes are very small. We neglect surface currents in our flux computations (i.e. take $U=w_a$ in eqs 1,2). The effect of currents on fluxes is generally small (Cornillon and Park. 2001), except in regions of weak mean winds and strong currents (e.g. under the ITCZ, where neglecting currents can induce latent heat flux errors ~7 Wm^{-2}, Jiang et al. 2005; Kelley et al. 2001). The telemetered daily wind speed data is computed from the daily averaged zonal and meridional wind components, rather than from 10-min wind speed time series (Cronin et al. 2006). As we will see later (section 4), neglecting the higher frequency (shorter than one-day) wind fluctuations results in an underestimation of wind speed (gustiness).

Daily turbulent heat fluxes at the mooring sites are selected only when all input variables (T_a, Q_a, W_a, SST) with 1 or 2 quality flags are available from the moorings. Figure 1a shows the number of valid daily data for which turbulent fluxes can be computed at each mooring location. More than 7 years of data are available at most sites in the Pacific Ocean, while only a few years are available in the Atlantic and Indian Oceans. A large number of moorings in the TPR array (although not all) are equipped with downwelling shortwave radiation sensors (Figure 1b), in particular in the Indian and Atlantic Oceans, as well as in the western Pacific and along 95°W. On the other hand, downwelling longwave radiation measurements are less numerous, and long records are only available at a few sites (Figure 1c). Estimates of daily air-sea fluxes from the above variables are available through the TAO project OceanSITES page at http://www.pmel.noaa.gov/tao/oceansites/index.html. We use these daily air-sea flux products for evaluating various flux products. A complete description of how they are obtained can be found in Cronin et al. (2006).

We retain only records with more than 6 months of 1 or 2 quality flags data, for all basic meteorological variables from the TPR moorings over the 2000-2009 periods. We chose 2000 as the beginning of our evaluation period because it is the date when the TPR array becomes stable in terms

of the daily average number of quality observations available for both turbulent heat flux computations (about 50) and downwelling shortwave radiation (about 30, see Fig. 2). Downwelling longwave radiations measurements are also available from early 2000 onward. Very similar evaluation statistics are obtained when computed over the longest possible period for each dataset, or the longest common period to all datasets.

Since this paper is concerned with the use of flux products to study intraseasonal to interannual climate variability, we apply a 5-day moving average to both the TPR data and evaluated data before computing the statistics (we hence only use points with more than 5-days of consecutive high quality data in our statistics). We interpolate the reanalysis data and satellite data to the TPR buoy location. We compute all the basic evaluation statistics (bias, correlation, rms-difference, ratio to observed standard deviation) separately for each data product at each mooring location. We then present the average of these statistics for all the locations, to avoid giving too much weight to the long datasets in the Pacific Ocean. Evaluation of the net heat flux is limited by the sparse availability of downwelling longwave radiation measurements. Since longwave heat fluxes contribute only a small fraction of net heat flux variability, we will present some net heat flux evaluation by using a common longwave radiation estimate for all products.

d. Independent validation datasets

It should be noted that the TPR dataset is not an independent validation dataset, for two reasons. First, TPR data is used directly or indirectly in most re-analyses or flux product that we evaluate here. Secondly, we will use TPR data in order to derive simple correction methods and construct the TropFlux product. For these reasons, we also need to compare the various flux products to other, more independent dataset.

The International Comprehensive Ocean-Atmosphere Data Set (ICOADS) offers simple gridded monthly summary products of marine data for 1° latitude x 1° longitude boxes since 1960 (Woodruff et al. 2010). While a large portion of this marine data has been used in the various re-analyses used in this paper (NCEP, NCEP2, ERA-I), we did not use ICOADS data to derive the bias and amplitude corrections applied to TropFlux input data. We hence used ICOADS data input variables (air temperature, humidity, wind speed, shortwave and longwave radiation) as an additional semi-independent evaluation of the meteorological parameters in this paper. In doing so, we excluded any data within 100 km of any TPR mooring location, in order to benefit from a highly independent evaluation to the one with TPR data. The ICOADS data won't allow validation of high frequency (~daily) variations (we use the monthly summary files), but at least allows to examine potential biases at locations distinct to those of the TPR network.

While the data above is not fully independent, we also used mooring data collected over the last two decades by the Woods Hole Oceanographic Institution (WHOI). These data were withheld from operational data streams in order to provide really independent data for validation of our products (ref). We use data from five experiment sites (see figure 1c for location and Table 2 for details): Arabian Sea experiment (Arabian Sea Mixed Layer Dynamics Experiment; Weller et al. 1998), COARE experiment (Coupled Ocean-Atmosphere Response Experiment; Webster and Lukas. 1992), WHOTS experiment (WHOI Hawaii Ocean Timeseries Station Experiment; ref), Stratus experiment (Colbo and Weller. 2007) and Subduction experiment (Brink et al. 1995) – which are located at contrasted and climatically relevant locations. Fluxes were computed at each site from hourly data and then averaged to daily values for comparison with the products in this paper.

When comparing the products to TPR or ICOADS data, which are not entirely independent, we will in the following refer to "evaluation" of the data. On the other hand, we will mention "validation" when comparing the various products to the independent WHOI flux data.

3. Evaluation of state variables and Correction methods

The parameters needed for turbulent fluxes computation using bulk formulae are: T_a, Q_a, SST and W_a. In this section, we will evaluate these parameters from several sources (NCEP/NCAR, NCEP2, ERA-I, OAFlux and satellite) with semi-independent TPR observations and then explain the corrections applied to ERA-I data to derive TropFlux turbulent fluxes.

a. Evaluation of state variables

Sea Surface Temperature. The SST variability is quite well captured by all products with high correlations (~0.9) and small biases (less than 0.11°C).

Air temperature. ERA-I air temperature has better correlation (> 0.9) than other air temperature products, but it does experience the largest bias (~ -0.28°C) and a slight underestimation of its variability (only 92% of observed standard deviation of 5-day smoothed data). All products tend to underestimate air temperature variability. NCEP and NCEP2 re-analyses have lowest correlation (~ 0.7) and strong systematic bias (-0.15°C and 0.18°C respectively).

Specific humidity. Humidity has the least well-reproduced variability amongst all parameters (Fig. 3a). As for temperature, ERA-I displays the best correlation (~0.85) but a large dry systematic bias compared to other products (~ -0.8 kg/kg). More than half of this dry bias (~ 55%) in ERA-I is related to the cold bias in air temperature, the remaining resulting from bias in relative humidity. Generally, all products considered here underestimate the mean humidity and the amplitude of its variability. OAFlux however displays the smallest rms error and NCEP has the least systematic bias.

Wind speed. ERA-I, OAFlux and Qscat wind speeds all capture the wind phase relationship against observations quite well, with correlation exceeding 0.9 (Figure 3a). NCEP and NCEP2 do not perform so well with correlation around 0.7 and 0.8 respectively. Reanalysis winds are always weaker than TPR winds, with ERA-I winds showing the largest negative bias (~ -0.3 m/s), while OAFlux and Qscat both overestimate the observed wind speed (~ 0.4 m/s). Wind speed variability is overestimated in NCEP/NCAR, and underestimated in ERA-I, OAFlux and Qscat. ERA-I shows the least rms error.

The above-described evaluation results reveal that ERA-I near surface variables display highest correlations with TPR data, despite caveats such as large T_a and Q_a bias and slightly underestimated variability. Our strategy is hence to derive *ad-hoc* bias and amplitude corrections for ERA-I, and then use these corrected variables to derive surface heat fluxes using COARE v3.0 algorithm

In the following section, we will describe our methodology for correcting the systematic bias and amplitude of variability for the ERA-I state variables.

b. Strategy for bias and amplitude correction

We correct the various variables used for heat flux computations using:

$$V^*(x,y,t) = a_V\left(V'(x,y,t) - \mathbf{V}(x,y)\right) + b_V(x,y) + \mathbf{V}(x,y), \qquad (8)$$

where V^* represents the corrected variable V, $\mathbf{V}$ is the long term mean of V, a_V is the amplitude correction, b_V is the bias correction. We describe below how we estimate a_V (which is always spatially homogeneous) and b_V (that can either be a constant or spatially variable).

Figure 4 shows the scatter plot of ERA-I systematic bias against climatological ERA-I value of SST, T_a, Q_a and W_a at each mooring. For SST, wind speed and specific humidity, no significant dependencies at the 99% level is noticed between the biases and mean ERA-I variables. In these cases, we use the mean systematic bias value over all the moorings as a spatially homogeneous bias correction. For air temperature, there is a clear dependency, which is significant at 99% confidence level. ERA-I shows larger negative bias at higher air temperatures and this trend becomes less evident at lower air temperatures. We therefore apply the following corrections to the original air temperature

$b_T(x,y) = -0.07 \times (\mathbf{T_a} - 22.6)$ for $22.6°C < \mathbf{T_a} < 28°C$

$b_T(x,y) = 0$ for $\mathbf{T_a} < 22.6°C$

$b_T(x,y) = 0.4$ for $\mathbf{T_a} > 28°C$

where b_T is the systematic bias correction and $\mathbf{T_a}$ the climatological ERA-I value. We use thresholds in order to avoid extrapolation of the corrections outside of the range that is well constrained by observations. We use this relation to derive a spatially variable bias correction from the climatological ERA-I temperature.

We did not find any statistically significant relation between the standard deviation ratio of ERA-I to observations and mean ERA-I values. A spatially uniform amplitude correction was hence applied to all variables on the basis of the ratio of the standard deviation of 5-day smoothed TAO data to 5-day smoothed ERA-I data. Note that a similar approach with un-smoothed data gives slightly larger amplitude corrections, and results in slightly degraded heat fluxes in comparison to mooring data. A possible reason for this may be an underestimation of high frequency variability (< 5 days) in the ERA-I re-analysis basic variables.

Our input data for computing heat fluxes are based on daily averaged data, over a 0.75° horizontal grid. This spatial and temporal averaging underestimates wind mesoscale variability, and will hence miss some of the flux variability. A classical approach to parameterize this is to apply a "gustiness" correction to the wind, in order to account for meso-scale flux enhancement. Various studies put forward different parameterization schemes for this gustiness correction (Zeng et al. 2002; Redelsperger et al. 2000). Making use of the high frequency hourly wind speed data available at the mooring locations, Cronin et al (2006) derived values for the gustiness correction based on the wind differences between daily and average high resolution wind data for each TPR mooring, which is used in the TPR turbulent flux calculation. Figure 5 shows the scatter plot of Cronin et al (2006) climatological gustiness values used against mean ERA-I SST values. There is a clear dependency of the gustiness to climatological SST (correlation of 0.8, significant at the 99% level) that can be approximated by the following formulae:

$$\Delta w_a = 0.18\ (\mathbf{SST} - 18.1) \text{ for } 23.7°C < \mathbf{SST} < 29.8°C$$

$$\Delta w_a = 1 \text{ for } \mathbf{SST} < 23.7°C$$

$$\Delta w_a = 2.1 \text{ for } \mathbf{SST} > 29.8°C$$

where Δw_a is the climatological gustiness correction and **SST** is the long term average ERA-I sea surface temperature value. The use of a minimum 1 m s^{-1} value for gustiness is motivated by the fact that Figure 3 of Zeng et al. (2002) never find any smaller value. The dependency of gustiness to SST reflects the more frequent occurrence of convective mesoscale systems at higher temperatures (e.g., Esbensen and McPhaden, 1996). We use this relation to derive a spatially variable gustiness wind correction from the climatological ERA-I SST.

c. Evaluation of the error correction strategy

By construction, the bias correction strategy above is improving the agreement between TropFlux and TPR data. In order to check that the correction strategy works at other locations than those of the TAO mooring, we show here comparisons to I-COADS monthly data. We masked data at all TPR mooring locations, thus effectively retaining ship and drifting buoy observations. Comparisons with these data will help to know how various sources of meteorological variables reproduce the variability at lower frequency time scales (higher than monthly scales.)

All products for all variables have very comparable correlations (not shown), suggesting that at lower frequencies (monthly and longer timescales) all products tend to capture the variability in a comparable way. Figure 6 shows the root mean square difference of various products for various meteorological variables against ICOADS observations. First, it can be seen that our correction strategy results in a smaller rms-difference to ICOADS observations for TropFlux than for ERA-interim. Our approach is hence successful in reducing the ERA-interim meteorological variables error at all locations, and not only at the TPR sites. OAFlux and TropFlux generally display the smallest rms-difference to ICOADs data, although the differences with other datasets remain relatively modest for SST, Ta and Qa. The TropFlux product however displays the best agreement to I-COADS monthly data in term of wind speed.

Another limit of our correction strategy (for both bias and variability amplitude) is that, except for sea surface temperature, a uniform bias correction was applied on the basis of comparison with TPR data. A uniform amplitude variability correction was also applied for all variables. Re-analysis estimates however possess spatially variable biases: e.g., Jiang et al. (2005) showed using two year TAO measurements that NCEP specific humidity Q_a tends to be too dry in the east and too wet in the west of Pacific. Repeating evaluation against ICOADS and TPR observations separately for the eastern Pacific, western Pacific, eastern Atlantic, western Atlantic and Indian Ocean (not shown) however shows that our correction improves the agreement with observations for all these regions.

4. TropFlux: a new near real time daily heat flux product for the Global Tropical Oceans.

In this section, we first evaluate NCEP, NCEP2, ERA-I, OAFlux and turbulent fluxes resulting from the correction strategy of section 3. We then evaluate existing radiative fluxes and describe our strategy for TropFlux radiative fluxes. Finally, we evaluate the resulting net heat fluxes from all the products against TPR observations.

a. Turbulent Flux

Figure 7 summarizes the evaluation of various turbulent flux products against TPR fluxes. Generally, the variability in latent heat flux is better reproduced than in sensible heat flux with higher correlation for the former in all products. The quality of latent and sensible heat fluxes reflect the quality of surface parameters discussed in section 3a. NCEP re-analyses have the worst performance (correlation of ~0.65 for latent and ~0.3 for sensible heat flux). NCEP2 has a large systematic error in heat flux (dry boundary layer resulting in a ~25 W m^{-2} overestimation of latent heat flux) while error compensation (dry boundary layer but weak wind) results in a weak bias in NCEP. OAFlux compares well with TPR moorings with quite high correlation and weak bias, but it tends to underestimate the observed variability.

The relatively high quality of ERA-I input parameters results in a realistic variability of ERA-I turbulent fluxes (correlation ~ 0.6 for sensible and ~ 0.8 for latent heat flux), but the strong biases in air temperature and humidity discussed earlier results in strong biases in turbulent fluxes (latent heat fluxes are overestimated by ~ 17 W m^{-2} and sensible fluxes by ~3 W m^{-2}). Applying the corrections described in the previous section to ERA-I parameters results in improved TropFlux turbulent flux variability (clearest for the sensible component) and a clear decrease of mean systematic bias. In general, OAFlux and TropFlux agree best with TPR data (with slightly larger biases for TropFlux LHF).

b. Surface Net Longwave Radiation (LWR)

In this section, we evaluate the net surface longwave radiation from NCEP, NCEP2, ERA-I, ISCCP and those estimated from the Clark et al. (1974) formula against TPR observations. Based on this, we will propose a strategy to derive a timely, high quality net surface longwave radiation for TropFlux.

The two NCEP re-analyses do not reproduce observed LWR well, with ~0.3 to 0.4 correlation and ~ 5 W m^{-2} systematic biases (Figure 8). The Clark et al. (1974) formula results in a reduced systematic bias (Figure 8d) but does not improve correlations to observed values (~0.4) and strongly underestimates amplitude of variability (about 65% of observed standard deviation). ISCCP estimates of net surface longwave radiation are better, with correlation higher than 0.6 and low bias, but they suffer from strongly overestimated variability and high rms-difference with observations. ERA-I LWR has the highest correlation (close to 0.7) and lowest rms-difference from observations, but underestimates the amplitude of the variability (~80% of that observed) with a ~5 W m^{-2} systematic bias. This overestimated upward longwave radiation flux may be related to the dry boundary layer (i.e. a weaker greenhouse effect in the near surface layer).

Since ERA-I LWR is a timely product and compares well with observations in terms of correlation, we applied the method described in section 3b to correct it for the mean systematic bias and reduced variance. Since there is no statistically significant relation between ERA-I LWR systematic bias and mean ERA-I values, we applied a constant bias correction of 4.6 W m^{-2} and a multiplicative coefficient a_{LWR} of 1.31 (=1/0.76) to the ERA-I LWR data. The resulting TropFlux net LWR corrects the two main issues of ERA-I (with very weak systematic bias and a variance close to TPR observations.

c. Surface Net Shortwave Radiation (SWR)

In this section, we evaluate the net surface shortwave radiation from NCEP, NCEP2, ERA-I and ISCCP, and propose a strategy to derive a timely net surface shortwave radiation for TropFlux.

As for LWR, the two NCEP re-analyses SWRs have serious issues with low correlation (~0.4), highest rms-difference (40 W m^{-2} or more) and strong systematic bias. ERA-I performs better than the two NCEP re-analyses but does not reproduce the observed variability as well as ISCCP (correlation of 0.7 against more than 0.85 for ISCCP). The correction approach described in 3b does not improve the correlation with observations, but is efficient in correcting the systematic bias and variance underestimate as in the ISCCP product. Our strategy is hence to use ISCCP data to estimate net surface SWR. Since the ISCCP SWR product is currently available only until 2007, we will describe in section 4d our strategy to extend ISCCP data to near-realtime to obtain a timely surface flux product.

We found a statistically significant relation between the record-mean ISCCP SWR and its bias at mooring locations (Figure 9). ISCCP SWR tends to be overestimated at lower mean-record values (e.g. by ~18 W m^{-2} for a climatological SWR of ~200 W m^{-2}). We therefore apply the following corrections to the original ISCCP SWR:

$$b_{SWR}(x,y) = 0.19 \times (\mathbf{SWR} - 295.4) \text{ for } 200\text{W m}^{-2} < \mathbf{SWR} < 295.4\text{W m}^{-2}$$

$$b_{SWR}(x,y) = 0 \text{ for } \mathbf{SWR} > 295.4\text{W m}^{-2}$$

$$b_{SWR}(x,y) = -18.4 \text{ for } \mathbf{SWR} < 200\text{W m}^{-2}$$

where b_{SWR} is the systematic bias correction and **SWR** the climatological ISCCP value. We use this relation to derive a spatially variable bias correction from the climatological ISCCP SWR.

There is no clear dependency of the ratio of standard deviation of ISCCP SWR with its mean values. We hence applied a constant variability correction a_{SWR} of 1.11 to the ISCCP anomalies. The corrected TropFlux SWR has by construction identical correlation values to ISCCP, but the

systematic error has been reduced from ~12 W m^{-2} to near zero and the rms difference is now lowest amongst all products (Figure 8).

d. Surface Net Shortwave Radiation (SWR) -Near Real Time

One issue in selecting ISCCP SWR product is that it is not a timely product (available only up to 2007 at the time of writing). This also restricts the timeliness of OAFlux since OAFlux relies on ISCCP for radiative fluxes. Since we want to obtain a timely estimate of the net heat flux, we provide an option to extend the ISCCP-corrected SWR to near real time as described below.

A better alternative than simply use corrected ERA-I SWR data to fill the time series relies in using OLR for SWR reconstruction (Shinoda et al. 1998; Sengupta et al. 2001). Shinoda et al (1998) obtained directly an estimate of SWR linearly from OLR (as SWR=0.93*OLR-1.03). This empirical relationship was modified by Sengupta et al (2001a,b) in order to adjust the problems in Shinoda's method in off-equatorial warm pool regions. (SWR=$\mathbf{SWR_{ERBE}}$+0.93*OLR_A, where $\mathbf{SWR_{ERBE}}$ is the climatological surface net insolation from Earth Radiation Budget Experiment and OLR_a is daily OLR anomaly). There is indeed a very good agreement of daily OLR interannual anomalies with SWR interannual anomalies from ISCCP (Figure 10). This agreement is, however, limited to warmer waters, with a correlation exceeding 0.7 above climatological SST of ~27°C. This good relationship reflects the fact that surface SWR is largely controlled by deep atmospheric convection over warmer water (of which OLR is a good indicator). On the other hand, low-level clouds play a strong role in modulating near-surface shortwave radiation over colder water (Cronin et al, 2006). Despite the good phase agreement described above, there is an underestimation of the amplitude of OLR anomalies with respect to mooring SWR anomalies (about 75% of observed standard deviation).

We followed a slightly different approach from Sengupta's method to calculate timely SWR: SWR=$\mathbf{SWR_{TropFlux}}$ +1.32*OLR_a where $\mathbf{SWR_{TropFlux}}$ is the TropFlux SWR daily mean seasonal cycle as described above (i.e. ISCCP mean seasonal cycle with both systematic bias and amplitude correction applied as described above) and OLR_a are the OLR daily interannual anomalies. Here, we applied a constant variability correction since we didn't find any statistically significant relationship between ratio of standard deviation of OLR and SWR anomalies against mean TropFlux SWR values. In the following sections, we will refer to the OLR-derived TropFlux SWR as "NRT" (for near real-time) and to the ISCCP- derived TropFlux SWR as "DT" (for delayed time).

Figure 8 shows the evaluation statistics of the TropFlux NRT SWR (here computed over 2000-2007 period). While it does not perform as well as the more elaborate ISCCP SWR estimate, this timely estimate performs better than any other re-analysis products (correlation of ~0.79, with reasonable amplitude and weak systematic bias). The NRT TropFlux SWR performs almost as well

as ISCCP or TropFlux over warm water (Table 4), as expected from Figure 10. Table 4 shows that, although it does not perform well over colder waters, the NRT SWR still clearly outperforms the re-analyses (NCEP, NCEP2 and ERA-I; see Table 4). Figure 11 further illustrates this by showing the correlation of TropFlux NRT SWR to mooring data, compared to ERA-I (the best of the re-analyses analyzed here, the others are not shown). Whereas TropFlux NRT SWR suffers from the same drawbacks than most re-analyses (which performs poorly over upwelling regions), it display better correlation with mooring data at almost all sites. Other statistics (rms-error, bias, standard deviation ratio: not shown) confirm that the TropFlux NRT SWR is better than any re-analysis product at almost all mooring sites.

At the time of writing, the TropFlux "delayed mode" (DM) SWR estimates are available until the end of 2007. The TropFlux timely SWR dataset based on OLR anomalies hence provides a viable option for extending the delayed mode TropFlux SWR data to near realtime.

e. Net flux

In this section, we will evaluate the net surface heat flux from various sources against TPR net fluxes. The average net flux evaluation statistics for all mooring locations within 30°N -30°S band, where net heat fluxes are available over the period 2000-2007 are summarized in figure 12. As expected, the NCEP and NCEP2 re-analyses show the worst performance with correlation of ~ 0.5 and rms-difference of more than 50 W m^{-2} to observations. In addition, both NCEP products suffer from a negative systematic bias (the ocean looses too much heat). As far as surface heat fluxes are concerned, NCEP2 is worse than NCEP with stronger bias and overestimated flux variability amplitude.

The ERA-I re-analysis performs considerably better than NCEP re-analyses with correlation of ~ 0.75 and rms-difference of ~ 40 W m^{-2} compared to observations, but it still displays a non-negligible -15 W m^{-2} systematic bias. The OAFlux/ISCCP net heat fluxes are of very good quality with correlation of ~ 0.82 and rms-difference of ~33 W m^{-2} compared to observations, but it still also displays a non-negligible +15 W m^{-2} systematic bias. The TropFlux product achieves a better comparison with observations (correlation of 0.85, systematic bias of ~ -2 W m^{-2} and rms-difference of 27 W m^{-2}), although the clearest improvement compared to OAFlux is in terms of the systematic bias.

As we pointed out in the introduction, actual estimates of LWR are not available at a lot of mooring sites. In order for our evaluation statistics to be more representative, we also tried to use a common LWR estimate (TropFlux LWR) for all products in the evaluation. When doing so, overall statistics that are obtained are not strikingly different from Figure 12, suggesting that, although based

on a limited number of samples, this figure is quite representative of the quality whole dataset. Table 5 shows the statistics separately for each ocean, and shows an equivalent level of performance in all three tropical oceans (with maybe more systematic bias in the Indian Ocean). The statistics have been presented in this paper for 5-day smoothed values, but the correlation with net heat flux "observations" from the TPR array remain very high (0.8) for daily values, suggesting a quite high level of consistency with TPR data for the TropFlux product.

5. Comparison between flux products

In this section, we will first provide a validation of the flux products considered in this paper (NCEP, NCEP2, ERA-I, OAFlux, TropFlux) to independent mooring data. Then we will show how these products are capturing El-Niño interannual variations in the Pacific and Madden Julian Oscillation (MJO) intraseasonal variations in the Indian Ocean.

a. Validation

As pointed out earlier, TPR observations do not provide an independent validation of various flux products because; (1) they are assimilated in various re-analysis and (2) TPR observations are used for deriving the *ad-hoc* corrections used in TropFlux data sets. In this section, we will compare the shortwave, latent and net fluxes from NCEP/NCAR, NCEP2, ERA-I, OAFlux/ISCCP and TropFlux with observations from five flux mooring sites described in section 3b. These data were withheld from operational data streams specifically for validation purposes, and were not used when deriving TropFlux corrections. The validation statistics provided in figure 13 are for daily values. We provide validation for the two most variable components of the net flux in the tropics (latent and shortwave), and for the net flux.

At all locations, the NCEP2 product display lowest correlation to independent LHF estimates (0.65 to 0.75), and almost always one of the strongest biases. NCEP LHF correlation is better, and almost equivalent to other products, but NCEP also displays one of the strongest biases at all locations. ERA-I is the re-analysis that generally displays the highest correlation with independent mooring LHF data, but it also suffers from significant bias at all locations. In general, the OAFlux and TropFlux products both exhibit some of the highest correlation to the validation dataset, and the least bias (the WHOTS site being the only one where TropFlux only ranks third in term of bias).

In terms of SWR, this comparison to independent data also seems to confirm conclusions drawn from the comparison to TPR data. First, re-analysis products in general perform poorly at reproducing observed daily SWR variations. Even our simple NRT SWR estimate performs generally better than re-analysis products, even above cold water (e.g. the Stratus site). The ISCCP

product (used in both OAFlux and TropFlux) consistently shows the best agreement to observed variability. In terms of bias, every product exhibit significant biases at given locations, except maybe ISCCP that consistently shows lower bias at all locations.

The resulting performance in terms of net heat flux also confirms result inferred from the comparison to TPR "dependent" data. NCEP and NCEP2 have issues, with both lowest correlations to independent net heat flux data and some of the strongest biases (despite some error compensations diminishing NCEP2 biases). ERA-I has generally quite a good correlation to observed data, but also suffers from comparatively strong biases at several sites. The TropFlux and OAFlux products both benefit from the highest correlation and comparatively smaller biases at all locations (except, maybe, in low level clouds regions where the TropFlux product suffers from systematic bias). Comparison of our near real time SWR and net fluxes also indicates that we are able to provide a near real time extension of the net fluxes without compromising much the quality of the data. This is really an advantage over OAFlux/ISCCP, since net flux from OAFlux/ISCCP is available only until 2007.

b. Flux variability

We will now illustrate the capacity of the TropFlux product to capture climate variations in the tropical regions by illustrating the surface flux signature of two widely studied phenomena: the Madden-Julian Oscillation (MJO) and El Niño. This will also allow us to illustrate the properties of various products over two contrasted regions: the Indian Ocean Warm pool and the eastern Pacific cold tongue.

One of the regions of strongest SST response to the Madden-Julian Oscillation in Boreal winter is the 60°-90°E, 5°-10°S region (Duvel and Vialard, 2007). Observations (Vialard et al. 2008) and modeling studies (Jayakumar et al. 2011) both suggest that net heat flux forcing is the largest contributor to the SST response in this region. How do the various heat flux products reproduce the net heat flux perturbations associated with the MJO in this region? Figure 14 show the average OLR (a good indicator of the local activity of the MJO), raw and 30-90 day filtered net heat fluxes in this region. There are particularly strong deep atmospheric convection perturbations in early 1999, 2000, 2001 and 2002 (figure 15a), which resulted in strong SST signature as reported in Vialard et al. (2009) and Duvel and Vialard (2007). There are rather strong mean heat flux differences between all products, with NCEP and NCEP2 on one end (lowest net heat flux into the ocean), OAFlux and TropFlux on the other end (strongest heat flux into the ocean), and ERA-I in the middle. There is however a striking similarity in the variability of all products at the intraseasonal timescale (Figure 14c), which shows an excellent, phase agreement between all products, and a good amplitude

agreement (only NCEP2 seems to clearly overestimate the MJO surface flux signature in this region).

Surface heat fluxes are known to be an important negative feedback to El Niño development in the cold tongue of the eastern Pacific (e.g. Wang and McPhaden, 2000; Vialard et al. 2001). Figure 15 shows the average SST anomaly (panel a), net heat fluxes (panel b) and heat fluxes interannual anomaly (panel c) over the Niño3 region (90°W-150°W, 5°S-5°N). There are even larger mean net heat flux differences over the cold tongue than the Indian Ocean warm pool. In addition to these differences, there are also very clear differences in seasonal cycle, with a tendency of the three re-analysis products to have smaller amplitude seasonal cycle with a pronounced semi-annual component (Cronin et al. 2006). Finally, though most products display a negative feedback of surface fluxes on El Niño (see the negative correlation between figure 15a and 15c), there are marked differences in the details of the variability of each product (see for example the spread in the net surface flux anomalies during the 1997-98 El Niño event). Even the two "best" products (on the basis of the evaluation made in this paper) OAFlux and TropFlux show non-negligible differences over this period (e.g. TropFlux has a standard deviation of 9 Wm^{-2} against 13 Wm^{-2} for OAFlux / ISCCP).

In summary, the various heat flux products evaluated in this paper seem to provide a quite consistent estimate of intraseasonal air-sea flux perturbations associated with the MJO in the Indian Ocean, but do exhibit clear mean state, seasonal cycle and interannual variability differences over the cold tongue in the eastern Pacific.

5. Summary and Discussion

a. Summary

The purpose of this paper is to evaluate several timely, daily air-sea flux products (NCEP, NCEP2, ERA-I and OAFlux/ISCCP) against observational estimates. We have also developed a new air-sea flux product, named TropFlux, for the global tropical oceans. This product is derived from ERA-I surface meteorological variables and longwave radiation, ISCCP shortwave radiation and NOAA OLR. TropFlux consists of all the four components of net heat flux and corrected near surface parameters like air temperature and air humidity at 2m heights, 10m-wind speed and Sea Surface Temperature (SST). TropFlux is available at a daily resolution on a 1° x 1° within 30°S-30°N via Internet at *[the http address will be confirmed when the paper gets accepted]*. TropFlux is available from 1989 to about 4 months behind the present, and will be updated on a monthly basis.

Evaluation of basic variables used as input for bulk turbulent flux estimates (sea surface temperature, air temperature and humidity at 2m height and wind at 10m height) reveals that the recently released ERA-Interim analysis product generally captures best the temporal variability (with correlations above 0.85 with TPR mooring data) despite strong systematic biases in surface temperature and humidity and an underestimation of variance. OAFlux also performs well in reproducing these parameters (correlation above 0.75 with weak systematic biases). On the other hand, both NCEP analyses have lower correlations and strong systematic biases relative to TPR observations.

The biases in individual components of the turbulent fluxes reflect those of the input parameters with ERA-I having good fidelity but strong systematic biases, OAFlux performing well, and both NCEP analyses performing worst. The longwave radiation data from all sources have low correlations with mooring observations (0.3 to 0.6) with ISCCP and ERA-I performing best. Shortwave radiation from the various re-analyses (correlations of 0.3 to 0.7) is generally inferior to those from ISCCP (which is correlated at ~0.85 with the observations).

We use mooring data to correct the systematic bias and amplitude of ERA-I input variables to compute TropFlux turbulent fluxes using the COARE v3.0 algorithm. Wind speed is also corrected to take mesoscale wind gustiness into account, based on the linear fit between climatological SST and gustiness values estimated from mooring data. Table 3 shows a summary of the corrections applied to each flux component. These corrections reduce considerably the systematic biases of ERA-I and result in turbulent fluxes of equivalent (or slightly better) quality than OAFlux when compared with TPR observations.

We use bias and amplitude corrected ERA-I surface net longwave radiation. Surface net shortwave radiation is based on ISCCP, with an amplitude and bias correction. The timeliness of the TropFlux product being limited by the availability of ISCCP SWR products, we extend the time series by using a “near real-time” SWR estimated from outgoing longwave radiation non-seasonal anomalies. The near realtime mode shortwave data performs well over convective regions but underestimates variability over the cold tongue. This “near real-time” estimate is however better than other reanalysis options, even over cold water. This near real-time data is used to complete the DT SWR time-series (i.e. from January 2008 to the end of 2009 at the time of writing).

The corrections applied for deriving TropFlux data were constructed solely on the basis of TPR data. It is hence important to check that they did improve the fit to observations away from TPR mooring locations. Comparison with monthly ICOADS observations at distinct locations than those of the TPR mooring array shows that our correction approach reduces rms-error for all input

parameters over the whole 30°N-30°S band. In addition, TropFlux and OAFlux display the smallest rms-errors to monthly ICOADS data amongst all datasets.

We have also compared all daily fluxes to fully independent daily flux data at 5 sites, sampling different climatic regimes. This independent validation seems to confirm inferences made from comparison with (dependent) TPR data. NCEP and NCEP2 exhibit both systematic biases and generally lower correlation to observations. While ERA-I generally displays a better temporal variability, but suffers from systematic biases. The best products are OAFlux/ISCCP and TropFlux, with correlations to TPR and independent flux estimates above 0.8 and systematic bias lower than 15 Wm^{-2}).

The various heat flux products evaluated in this paper seem to provide a quite consistent estimate of intraseasonal air-sea flux perturbations associated with the MJO in the Indian Ocean, but do exhibit clear mean state, seasonal cycle and interannual variability differences over the cold tongue in the eastern Pacific.

b. Discussion

The evaluations with TPR observations that we provide in this paper are not actual error estimates. First, they are comparisons relative to TPR data, which themselves suffers from observational errors. Second, the COARE algorithm only provides an indirect estimate of the air-sea fluxes, unlike more direct turbulent flux measurements. The target uncertainty for net heat flux daily estimates accuracy from the COARE v3.0 algorithm is 10 W m^{-2}. If one assumes that the COARE algorithm error and the one of our algorithm are independent, this results in a negligible increase of the rms-error estimates in Table 5 (from ~45 W m^{-2} to 46 W m^{-2}). The estimates in Table 5 are hence probably reasonable estimates of the accuracy of the products. Errors are hence dominated by input data (i.e., re-analysis) errors and by meso-scale variability (i.e. the fact that one compares a point estimate with an average over a ~100km per 100 km grid cell).

Our strategy for correcting the amplitude of input parameter variations relies on the assumption that the amplitude mismatch is the same at all timescales. In practice, it is quite likely that re-analysis products tend to be less accurate for high frequency variability (each “event” being constrained by only a few observations) than for low-frequency variability. A detailed analysis of the near-surface specific humidity and winds for example show that, although our method reduces mismatches in amplitude with TPR observations globally, it can locally result in slightly overestimated amplitude of the seasonal cycle (e.g. in the eastern Pacific).

This study provides a useful complement to the OAFlux dataset. Since OAFlux does not use ERA-I in its objective analysis and TropFlux is mainly developed from ERA-I, OAFlux and

TropFlux are partially independent. TropFlux hence provides partially independent daily air-sea fluxes available over a long period (since 1989 as against 1985 for OAFlux). This is clearly a necessity when considering the large discrepancies amongst even those two (TropFlux and OAFlux) products when it comes to, e.g., the mean seasonal cycle and interannual variability over the eastern Pacific cold tongue. Second, although the near real-time radiative flux option that we provide is not as good as ISCCP estimates, it provides a reasonable option for getting near-real time estimates across the global tropics. We provide both the corrected ISCCP shortwave (1989-2007), near real time-estimates (since 1989) and merged estimates (corrected ISCCP shortwave for the entire period over which it is available, and then near real-time estimates with a smooth 90-day linear transition between the two).

As a final note, we should stress the utmost importance of maintaining long-term time series of truly independent air-sea fluxes estimates at a few sample climatologically relevant sites. Only this type of fully independent data (withheld from meteorological centres data stream) can help to ensure the quality of available air-sea flux products.

Acknowledgements: The development of TropFlux product is the result of a joint research collaboration between National Institute of Oceanography (Goa, India) and Institute Pierre et Simon Laplace (Paris, France). BPK and VSNM thanks Director, National Institute of Oceanography, India, for his keen interest in this study. The lead author is supported by a Senior Research Fellowship (SRF) from Council of Scientific and Industrial Research (CSIR, Govt. of India) and a one-year research grant from Institut de Recherche pour le Développement (IRD, France) and did part of this work whilst at Laboratoire d'Océanographie Expérimentation et Approches Numériques (LOCEAN, Paris). JV and ML are funded by Institut de Recherche pour le Développement (IRD) and did this work while visiting National Institute of Oceanography (NIO, India). We sincerely thank the providers of NCEP, NCEP2 re-analyses and OLR data (NOAA/OAR/ESRL PSD, Boulder, Colorado, USA), ERA-Interim (European Centre for Medium Range Weather Forecasting), OAFlux (Woods Hole Oceanographic Institution), ISCCP (International Satellite Cloud Climatology Project), TMI SST (Remote Sensing Systems), Qscat winds (CERSAT-IFREMER) and TAO-PIRATA-RAMA (PMEL-NOAA) for various data sets. Meghan Cronin and Dai McClurg (PMEL) provided TPR climatological wind gustiness data. Discussions with Jean-Luc Redelsperger on wind gustiness parameterization provided useful inputs. Constructive comments by two anonymous reviewers greatly helped to improve an earlier version of this manuscript. This is NIO contribution number xxxx and PMEL contribution number 3628.

References

Anderson, A., S. Bakan, K. Fennig, H. Grassl, C-P. Kleep, J. Schlz, 2007: Hamburg Ocean Atmosphere Parameters and Fluxes from Satellite Data – HOAPS-3., electronic publication, World Data Centre for Climate, doi:10.1594/WDCC/HOAPS3_MOMTHLY.

Bentamy. A., K.B. Katsaros, A. Mestas-Nuñez, W. Drennan, E. Forde, and H. Roquest, 2003: Satellite estimates of wind speed and latent heat flux over the global oceans, *J. Climate*, **16**, 637-656.

Berry and Kent, 2009: A new air-sea interaction gridded dataset from ICOADS with uncertainty estimates, *Bull. Amer. Meteor. Soc.*, **90**, 645-656.

Bignami. F., S. Marullo, R. Santoleri, and M. E. Schiano, 1995: Longwave radiation budget in the Mediterranean Sea, *J. Geophys. Res*, **100** (C2), 2501-2514.

Bjerknes. J., 1966: A possible response of the atmospheric Hadley circulation to equatorial anomalies of ocean temperature, *Tellus*, **18**, 820-829.

Bolton, D., 1980: The computation of equivalent potential temperature. *Mon. Wea. Rev*, **108**, 1046-1055.

Bourassa, M. A., D. G. Vincent, and W. L. Wood, 1999: A flux parameterization including the effects of capillary waves and sea state, *J. Atmos. Sci*., **56**, 1123-1139.

Bourlès, B., R. Lumpkin, M. J. McPhaden, F. Hernandez, P. Nobre, E. Campos, L. Yu, S. Planton, A. J. Busalacchi, A. D. Moura, J. Servaom, and J. Trotte, 2008: The PIRATA Program : History, Accomplishments and Future Directions, *Bull. Am. Meteorol. Soc*., **89**, 1111-1125.

Bradley, E. F., C. W. Fairall, J. E. Hare, and A. A. Grachev, 2000: An old and improved bulk algorithm for air-sea fluxes: COARE2.6a. *AMS 14th Symposium on Bounday Layers and Turbulence*. Aspen, Colorado.

Brink, N. J., K. A. Moyer, R. P. Trask, and R. A. Weller, 1995: The Subduction Experiment: Mooring Field Program and Data Summary. Woods Hole Oceanographic Institution. WHOI-95-08, 113 pp.

Brunke, M. A., X. Zeng, and S. Anderson, 2002: Unceertainties in sea surface turbulent flux algorithms and data sets. J. *Geophys. Res*., **107**, 3141, doi:10.1029/2001JC000992.

Brunke, M. A., C. W. Fairall, and X. Zeng, 2003: Which bulk aerodybamic algorithms are least problematic in computing ocean surface turbulent fluxes? *J. Climate*, **16**, 619-635.

Budyko, M. I., 1963: Atlas of the Heat Balance of the Earth, *Kartfabrika Gosgeoltenizdata*, Leningrad.

Bunker, A. F., 1976: Computations of surface energy flux and annual air-sea interaction cycles of the north Atlantic, *Mon. Wea. Rev*., **104**, 1122-1140.

Bunker, A. F., Worthington, L. V, 1976: Energy exchange charts of the north Atlantic Ocean, *Bull. Amer. Meteor. Soc*., **57**, 670-678.

Cassou, C., 2008, Intraseasonal interaction between the Madden–Julian Oscillation and the North Atlantic Oscillation, *Nature*, **455,** 523-527.

Chiang, J. C. H., and D, J. Vimont, 2004: Analogues Pacific and Atlantic Meridional Modes of tropical atmosphere-ocean variability, *J. Clim*, **18**, 403-420.

Chou. S. H., E. Nelkin, J. Ardissone, R. M. Atlas, 2004: A comparison of latent heat fluxes over global oceans for four flux products. *J. Climate*, **17**, 3973-3989.

Clark, N. E., L. Eber, R. M. Laurs, J. A Renner, and J. F. T. Saur, 1974: Heat exchange between ocean and atmosphere in the eastern North Pacific for 1961-71. NOAA Tech. Rep. NMRS

SSRF-682, 108 pp.

Clayson, C. A., and J. A. Curry, 1996 : Determination of surface turbulent fluxes for TOGA COARE: Comparison of satellite retrievals and in situ measurements. *J. Geophys. Res*., **101**, 28 503-28 513.

Colbo, K., and R. Weller, 2007: The variability and heat budget of the upper ocean under the Chile-Peru stratus, *J. Mar. Res*, **65**, 607-637.

Cornillon, P., and K. –A. Park, 2001: Warm core ring velocity inferred from NSCAT, *Geophys. Res. Lett*, **28**, 575-578.

Cronin, M. F., C. Fairall, and M. J. McPhaden, 2006: An assessment of buoy-derived and numerical weather prediction surface heat fluxes in the tropical Pacific. *J. Geophys, Res*, **111**, C06038, doi:10.1029/2005JC003324.

Cronin, M. F., N. Bond, C. W. Fairall, and R. A. Weller, 2006: Surface Cloud Focrcing in the East Pacific Stratus Deck/Cold Tongue/ITCZ Complex. *J. Clim*, **19**, 392-409.

Curry, J.A., et al, 2004: SEAFLUX, *Bull. Am. Meteorol*. Soc., **85**, 409-424.

Dee, D. P., and S. Uppala, 2009: Variational bias correction of satellite radiance data in ERA-interim reanalysis. *Quart. J. R. Meteorol. Soc*., **135**, 1830-1841.

Duvel, J-P. and J. Vialard, 2007, Indo-Pacific Sea Surface Temperature Perturbations Associated with Intraseasonal Oscillations of the Tropical Convection, *J. Clim.*, **20,** 3056-3082.

Elms, J. D., S. D. Woodruff, S. J. Worley, and C. Hanson, 1999: Digitizing Historical Records for the Comprehensive Ocean-Atmosphere Data Set (COADS), *Earth System Monitor*, **4**(2), 4-10.

Esbensen, S.K. and M.J. McPhaden, 1996: Enhancement of tropical ocean evaporation and sensible heat flux by atmospheric mesoscale systems. *J. Clim., 9*, 2307-2325.

Fairall, C. W., E. F. Bradley, D. P. Rogers, J. B. Edson, and G. S. Young, 1996: Bulk parameterization of air-sea fluxes for Tropical Ocean-Global Atmosphere Coupled Ocean-Atmosphere Response Experiment. *J. Geophys. Res*., **101**, 3747-3764.

Fairall, C. W., E. f. Bradley, J. E. Hare, A. A. Grachev, and J. B. Edson, 2003: Bulk parameterization on air-sea fluxes : Updates and verification for the COARE algorithm. *J. Climate*, **16**, 571-591.

Foltz, G. R., and M. J. McPhaden, 2005: Mixed layer heat balance on intraseasonal time scales in the northwestern tropical Atlantic Ocean. *J. Climate*, **18**, 4168-4184.

Foltz, G. R., J. Vialard, Praveen Kumar B. and M. J. McPhaden, 2010 : Seasonal mixed layer heat balance of the southwestern tropical Indian Ocean, *J. Clim.*, **23,** 947-965.

Freitag, H.P., M.E. McCarty, C. Nosse, R. Lukas, M.J. McPhaden, and M.F. Cronin, 1999: COARE Seacat data: Calibrations and quality control procedures. NOAA Tech. Memo. ERL PMEL-115, 89 pp.

Freitag, H. P., M. O'Haleck, G.C. Thomas, and M.J. McPhaden, 2001: Calibration procedures and instumental accuracies for ATLAS wind measurements. NOAA. Tech. Memo. OAR PMEL-119, NOAA/Pacific Marine Environmental Laboratory, Seattle, Washington, 20 pp.

Grassl. H., V. Jost, R. Kumar, J. Schulz, P. Bauer, and P. Schluessel, 2000: The Hamburg Ocean Atmosphere Parameters and Fluxes from Satellite Data (HOAPS): A Climatological Atlas of Satellite Derived Air-Sea Interaction Parameters over the Oceans., Report No **312**, ISSN 0937-1060, Max Planck Institute for Meteorology, Hamburg.

Hendon, H. H., 2003: Indonesian Rainfall Variability: Impacts of ENSO and Local Air–Sea Interaction, *J. Climate,* **16,** 1775-1790.

Jiang, C., M.F. Cronin, K.A. Kelly, and L. Thompson, 2005: Evaluation of a hybrid satellite- and NWP-based turbulent heat flux product using Tropical Atmosphere-Ocean (TAO) buoys. *J. Geophys. Res.*, *110*(C9), C09007, doi:10.1029/2004JC002824.

Jayakumar, A., J. Vialard, M. Lengaigne, C. Gnanaseelan, J. P. McCreary, B. Praveen Kumar, 2010: Processes controlling the surface temperature signature of the Madden-Julian Oscillation in the thermocline ridge of the Indian Ocean, *Clim. Dynamics*, **in press**.

Josey, S. A., D. Oakely, and R. W. Pascal, 1997: On estimating the atmospheric longwave flux at the ocean surface from ship meteorological reports, *J. Geophys. Res*, **102**, 27961-27972.

Josey, S. A., Kent, E. C. and Taylor, P. K, 1999: New insights into the ocean heat budget closure problem from analysis of the SOC air-sea flux climatology, *J. Clim*, **12**, 2856-2880.

Kalnay et al.,1996: The NCEP/NCAR 40-year reanalysis project, *Bull. Amer. Meteor. Soc*, **77**, 437-470.

Kanamitsu, M., W. Ebisuzaki, J. Woolen, J. Potter and M. Fiorino, 2002: NCEP/DOE AMIP-II Reanalysis (R-2). *Bull. Amer. Met. Soc*. **83**, 1631-1643.

Kelly, K. A., S. Dickinson, M. J. McPhaden, and G. C. Johnson, 2001: Ocean currents evident in satellite wind data, *Geophys. Res. Lett*, **28**, 2469-2472.

Klein, S. A., B. J. Soden, and N.-C. Lau, 1999: Remote sea surface temperature variations during ENSO: Evidence for a tropical atmospheric bridge, *J. Clim*, **12**, 917-932.

Kubota, M., N. Iwasala, S. Kizu, and M. Knoda, 2002: Japanese Ocean Flux Data Sets with Use of Remote Sensing Observations (J-OFURO). *J. Oceanogr*., **58**, 213-215

Kummerow, C., W. Barnes, T. Kozu, J. Shiue, and J. Simpson, 1998: The Tropical Rainfall Measuring Mission (TRMM) sensor package. *J. Atmos. Oceanic Technol*, **15**, 809-816.

Lake, B. J., S. M. Norr, H. P. Freitag, and M. J. McPhaden, 2003: Calibration procedures and intrumental accuracy estimates of ATLAS air temperature and relative humidity measurements. NOAA Tech Memo. OAR PMEL-123, NOAA/Pacific Marine Environmental Laboratory, Seattle, WA, 23 pp.

Liebmann, B., and C. A. Smith, 1996: Description of a complete (interpolated) outgoing longwave radiation dataset. *Bull. Amer. Meteor. Soc*., **77**, 1275-1277.

Madden, and Julian, 1972: Description of global-scale circulation cells in the Tropics with a 40-50 day period. *J. Atmos. Sci*, **29**, 3138-3158.

McPhaden, M. J., A. J. Busalacchi, R. Cheney, J. R. Donguy, K. S. Gage, D. Halpern, M. Ji, P. Julian, G. Mayers,, G. T. Mitchum, P. P. Niiler, J. Picaut, R. W. Reynolds, N. Smith, K. Takeuchi, 1998: The Tropical Ocean-Global Atmosphere (TOGA) observing system: A decade of progress. *J. Geophys. Res*., **103**, 14,169-14,240.

McPhaden, M. J., S. E. Zebiak, Sand, M.H. Glantz, 2006: ENSO as an integrating concept in Earth science. *Science*, **314,** 1740-1745.

McPhaden, M. J., G. Meyers, K. Ando, Y. Masumoto, V. S. N. Murty, M. Ravichandran, F. Syamsudin, J. Vialard, W. Yu, L. Wu, 2009: RAMA: Research Moored Array for African-Asian-Australian Monsoon Analysis and Prediction. *Bull. Am. Met. Soc.*, **90,** 459-480.

Mears, C. A., D. K. Smith, and F. J. Wentz, 2001: Comparison of Special Sensor Microwave Imager and buoy-measured wind speeds from 1987 to 1997. *J. Geophys. Res*., **106**, 11, 719-11,729.

Medavaya, M., D.E. Waliser, R.A. Weller, and M.J. McPhaden, 2002: Assessing ocean buoy shortwave shortwave observations using clear-sky model calculations. *J. Geophys. Res.*, *107*(C2), 3014, doi:10.1029/2000JC000558.

Murtugudde, R., J. P. McCreary, and A. J. Busalacchi, 2000: Oceanic processes associated with anomalous events in the Indian Ocean with relevance to 1997-1998, *J. Geophys. Res*., **105**, 3295-3306.

Parekh, A., R. Sharma, and A. Sarkar, 2007: A comparative assessment of sea wind speed and sea surface temperature over the Indian Ocean by TMI, MSMR, and ERA-40. *J. Atmos. Oceanic Technol*, **24**, 1131-1142

Payne, R.E., K. Huang, R.A. Weller, H.P. Freitag, M.F. Cronin, M.J. McPhaden, C. Meinig, Y. Kuroda, N. Ushijima, R.M. Reynolds, 2002: A comparison of buoy meteorological systems. WHOI Technical Report WHOI-2002-10. Woods Hole Oceanographic Institution, 67 pp.

Perry, A. H., Walker, J. M, 1977: *The Ocean-Atmosphere System*. New York: Longman Inc., 160pp.

Redelsperger, J. L., F. Guichard, and S. Mondon, 2000: A parameterization of mesoscale enhancement of surface fluxes for large scale models. *J. Climate*, **5**, 402-421

Reed, R., 1977: On estimating insolation over the ocean. *J. Phys. Oceanogr*, **7**, 482-485.

Saji NH, Goswami BN, Vinayachandran PN, Yamagata T, 1999: A dipole mode in the tropical Indian Ocean. *Nature*, **401,** 360–363

Schulz, J., and S. Bakan, 1998: A new satellite-derived freshwater flux climatology (Hamburg Ocean Atmosphere Parameters and fluxes from Satellite data). *International WOCE Newsletter*, **32**, 20-26.

Sengupta, D., and M. Ravichandran, 2001: Oscillations of Bay of Bengal sea surface temperature during the 1998 summer monsoon. *Geophys. Res. Lett*, **28**, 2033-2036.

Sengupta, D., B. N. Goswami, and R. Senan, 2001: Coherent intraseasonal oscillations of ocean and atmosphere during the Asian summer monsoon. *Geopys. Res. Lett*, **28,** 4127-4130.

Shinoda, T., and H. H. Hendon, 1998: Mixed layer modeling of intraseasonal variability in the tropical western Pacific and Indian Oceans. *J. Clim*., **11**, 2668-2685.

Smith, S.D., 1988: Coefficients for sea surface wind stress, heat flux and wind profiles as a function of wind speed and temperature. *J. Geophys. Res*., **93**, 15,467-15,472.

Sobel, A.H., E.D. Maloney, G. Bellon and D.M. Frierson, 2008: The role of surface fluxes in tropical intraseasonal oscillations. *Nat. Geoscience*, **1,** 653-657.

Uppala et al. 2005. The ERA-40 re-analysis, *Quarterly Journal of the Royal Meteorological Society*, **131**, 2961-3012, DOI: 10.1256/qj.04.176.

Vialard, J., C. Menkes, J-P. Boulanger, P. Delecluse, E. Guliyardi, M. J. McPhaden, and G. Madec, 2001: A model study of oceanic mechanisms affecting equatorial Pacific sea surface temperature during the 1997-1998 El-Nino, *J. Phys, Oceanogr*., **31**, 1649-1675.

Vialard, J., G. Foltz, M. McPhaden , J-P. Duvel and C. de Boyer Montégut, 2008, Strong Indian Ocean sea surface temperature signals associated with the Madden-Julian Oscillation in late 2007 and early 2008, *Geophys. Res. Lett.*, **35,** L19608, doi:10.1029/2008GL035238

Vialard. J., A. Jayakumar, C. Gnanaseelan, M. Lengaigne, D. Sengupta, 2011: Processes of intraseasonal sea surface temperature variability in the Northern Indian Ocean during boreal summer *Clim. Dynamics*, **xxxxx**

Wang,W. and M.J. McPhaden, 2000: The surface layer heat balance in the equatorial Pacific Ocean, Part II: Interannual variability. *J. Phys. Oceanogr.*, *30*, 2989-3008.

Webster, P. J., Moore, A. M, Loschnigg, J. P, and Leben, R. R, 1999: Coupled oceanic-atmospheric dynamics in the Indian Ocean during 1997-98, *Nature*, **401**, 356-360.

Webster, P., and R. Lukas, 1992: TOGA-COARE The Coupled Ocean-Atmosphere Response Experiment. *Bull. Amer. Meteor*. **73**, 1377-1416.

Weissman, D. E., M. A. Bourassa and J. Tongue, 2002: Effects of rain rate and wind magnitude on SeaWinds scatterometer wind speed errors. Journal of Atmospheric and Oceanic Technology, **19**, pp. 738-746.

Weller, R. A., M. F. Baumgartner, S. A. Josey, A. S. Fischer, and J. Kindle, 1998: Atmospheric forcing in the Arabian Sea during 1994-1995: Observations and comparisons with climatology and models, *Deep-Sea Res*., **45**, 1961-1999.

Woodruff, S. D., S. J. Lubker, K. Wolter, S. J. Worley, and J. D. Elms, 1993: Comprehensive Ocean-Atmosphere Data Set (COADS) release la:1980-92, *Earth Syst. Monit*., **4**, 4-8.

Xie, S.-P., and J. A. Carton, 2004: Tropical Atlantic variability: Patterns, mechanisms, and impacts, in *Earth's Climate: The Ocean-Atmosphere Interacion, Geophys. Monogr. Ser*, vol.**147**, edited by C. Wang, S.-P. Xie and J. A. Carton, pp.121-142, AGU, Washington, D. C.

Xie, S. –P., and Philander, 1994: A coupled ocean-atmosphere model of relevance to the ITCZ in the eastern Pacific, *Tellus, Ser. A*, **46**, 340-350.

Yu, L., and R. A. Weller, 2007: Objectively Analyzed air-sea heat Fluxes (OAFlux) for the global oceans. *Bull. Ameri. Meteor. Soc*., **88**, 527-539.

Yu, L. S., R. A. Weller, and B. Sun, 2004a: Improving latent and sensible heat flux estimates for the Atlantic Ocean (1988-1999) by a synthesis approach. *J. Climate*, **17**, 373-393.

Yu, L. S., R. A. Weller, and B. Sun, 2004b: Mean and variability of the WHOI daily latent and sensible heat fluxes at in situ flux measurement sites in the Atlantic Ocean. *J. Climate*, **17**, 2096-2118.

Zeng, X., M. Zhao, and R. E. Dickinson, 1998: Intercomparison of bulk aerodynamic algorithms for the computation of se surface fluxes using the TOGA COARE and TAO data. *J. Climate*, **11**, 2628-2644.

Zeng, X., Q. Zhang, D. Johnson, and W. –K. Tao, 2002: Parameterization of wind gustiness for the computation of ocean surface fluxes at different spatal scales. *Mon. Weather Rev*, **130**, 2125-2133

Zhang, Y. C., W. B. Rossow, A. A. Lacis, V. Oinas, and M. I. Mishchenko, 2004: Calculation of radiative fluxes from the surface to top of atmosphere based on ISCCP and other global data sets: Refinments of the radiative transfer model and the input data. *J. Geophys. Res*., **109**, D19105, doi:10.1029/2003JD004457.

Zhang, C., M. Dong, S. Gualdi, H.H. Hendon, E.D. Maloney, A. Marshall, K. R. Sperber, W. Wang, 2006: Simulations of the Madden–Julian oscillation in four pairs of coupled and uncoupled global models. *Clim. Dyn.*, **27,** 573-592.

Data Product	Start date	Resolution	End date
NCEP/NCAR	01-01-1948	4 x daily	Near Real time
NCEP2	01-01-1979	4 x daily	Updated once per year
ERA-Interim	01-01-1989	4 x daily	3-4 months behind realtime
ERA-40	01-09-1957	4 x daily	31-08-2002
OAFlux (turbulent fluxes) ISCCP (radiative fluxes)	01-01-1985 01-07-1983	Daily Daily	Updated twice per year 31-12-2007
J-OFURO	01-01-1988	Daily	31-12-2006
HOAPS 3[@]	09-07-1987	2 x daily	31-12-2005

Table 1: List of major daily net heat flux dataset available for tropical regions.

Experiment	Location	Deployment period
Arabian Sea Experiment	15.3°N, 61.3°E	October 1994 to October 1995
COARE	1.45°S, 156°E	October 21, 1992 to March 4, 1993
Subduction experiment	Central buoy (25.5°N, 29°W); Southwestern buoy (18°N, 34°W) Southeastern buoy (18°N, 34°W)	June 1991 to June 1993
Stratus *	20°S, 85°W	Since October 2000
WHOTS *	22.4°5 N, 158°W	Since August 2004

Table2: list of flux estimates used for independent evaluation of various flux products.

* Validation is done with these data until 2007 in order to include a comparable comparison of OAFlux/ISCCP fluxes with other sources of datasets.

	Data source	Bias correction	Amplitude correction	Additional remarks
SST	ERA-I	Constant = 0.05	Constant = 1/0.98	
Wind	ERA-I	Constant = 0.28	Constant = 1/0.90	Gustiness correction estimated from climatological SST Δw_a = 0.18 (**SST** – 18.1) for 23.7 < **SST** < 29.8 Δw_a = 1 for **SST** < 23.7 Δw_a = 2.1 for **SST** > 29.8
Ta	ERA-I	Variable equation $b_T(x,y)$= -0.07 x ($\mathbf{T_a}$-22.6) for 22.6°C < $\mathbf{T_a}$ < 28°C $b_T(x,y)$= 0 for $\mathbf{T_a}$ < 2.6°C $b_T(x,y)$= 0.4 for $\mathbf{T_a}$ > 28°C	Constant = 1/0.92	
Qa	ERA-I	Constant = 0.79	Constant = 1/0.92	
LWR_{net}	ERA-I	Constant = -4.62	Constant = 1/0.76	
SWR_{net} (DT)	ISCCP	Mean seasonal cycle corrected from equation $b_{SWR}(x,y)$ = 0.19 x (**SWR** – 295.4) for 200W.m^{-2} < **SWR** <295.4W.m^{-2} $b_{SWR}(x,y)$ = 0 for **SWR** > 295.4W.m^{-2} $b_{SWR}(x,y)$ = -18.4 for **SWR** < 200W.m^{-2}	Constant = 1/0.90	
SWR_{net} (RT)	ISCCP	Seasonal cycle as above	As above	Provided to complete the net heat flux time series beyond the end of ISCCP radiative fluxes until near realtime.
	NOAA OLR	Interannual anomaly from OLRA	Constant = 1/0.76 on OLR_a	

Table 3. Summary of methods to estimate the TropFlux product

Location	SWR Source	Correlation	bias	Std ratio	rmsd
SST > 27°C	NCEP/NCAR	0.50	-12.91	0.56	40.22
	NCEP2	0.41	-16.37	1.11	52.34
	ERA-I	0.76	1.43	0.85	26.68
	ISCCP	0.86	13.07	0.90	24.09
	TropFlux	0.86	-1.54	1.00	21.31
	TropFlux_NRT	0.81	-0.94	0.94	24.42
SST < 27°C	NCEP/NCAR	0.43	-14.36	0.89	40.36
	NCEP2	0.38	-31.05	1.43	57.85
	ERA-I	0.64	7.76	0.85	26.42
	ISCCP	0.83	10.80	0.91	20.23
	TropFlux	0.83	0.24	1.01	18.34
	TropFlux_NRT	0.73	1.52	0.87	21.88

Table 4: showing the evaluation of net surface SWR from different sources against TPR observations over 2000-2007 period for climatological TPR SST above 27°C and SST below 27°C. The statistics shown are for 5 day averaged data.

	Cor	Bias	Std ratio	rmsd
Global (daily)	0.80	1.48	0.95	44.66
Global	0.85	1.48	1.02	30.68
Indian Ocean	0.87	-11.23	1.1	34.58
Pacific Ocean	0.84	5.04	0.99	30.23
Atlantic Ocean	0.85	3.63	1.01	28.73

Table 5: Table showing the evaluation statistics of TropFlux net heat flux against high quality TPR (quality flag 1 and 2) observations over the 1989-2009 period. A common LWR product (TropFlux LWR) is used for calculating TPR and TropFlux net heat flux. The numbers in this table represent the validation of the 5-day smoothed data, except the first line, which gives the statistics for daily products.

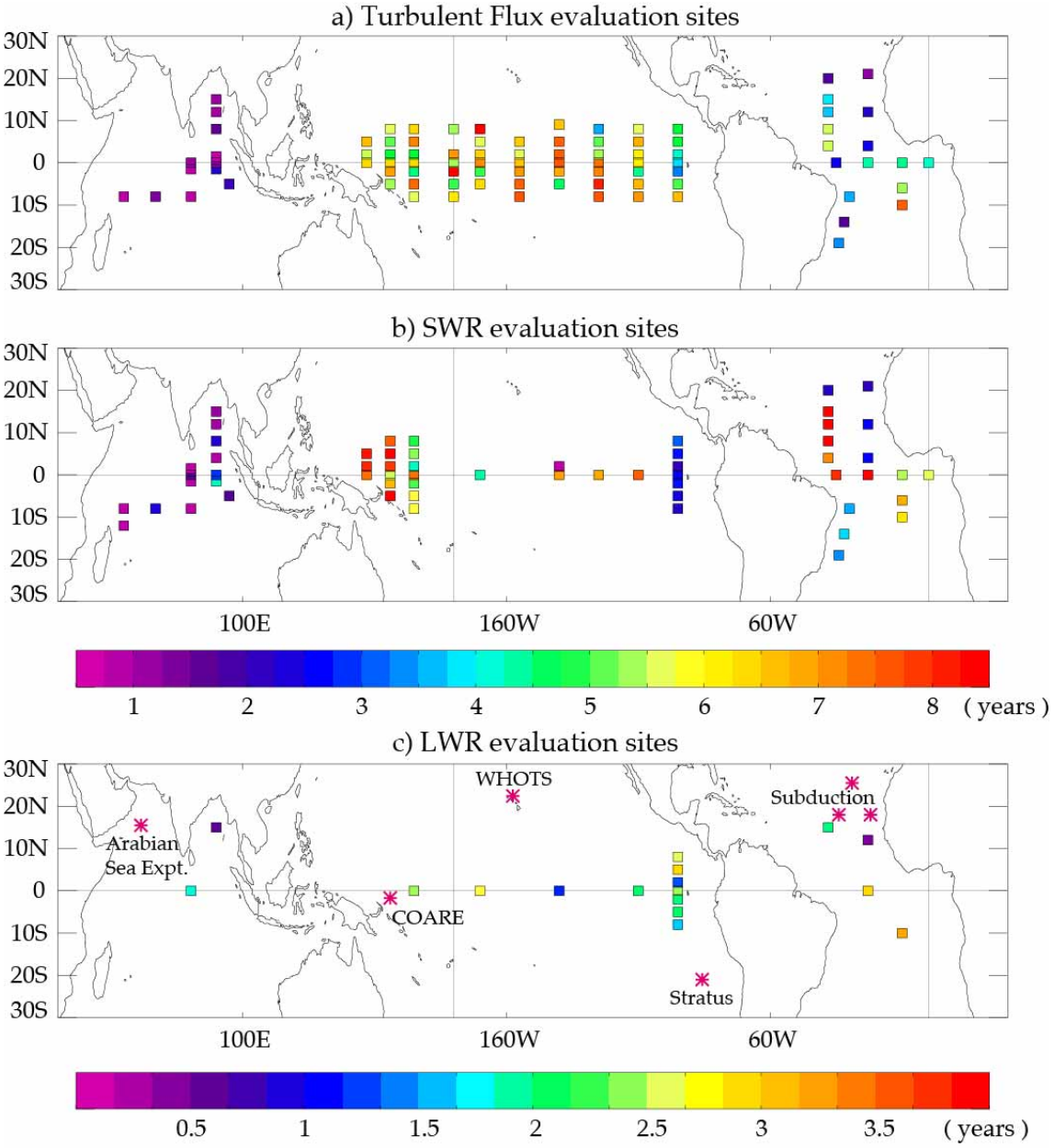

Figure 1. Total length (in years) of valid (quality flag 1 or 2) flux measurements from 2000 to 2009 at TAO/PIRATA/RAMA sites for a) turbulent flux estimates (SST, Ta, qa and wind must be available with best or standard quality flags); b) Shortwave radiation and c) Longwave radiation. Only locations with more than 180 days of high quality observations are shown here. Purple asterisks on panel c indicate independent validation sites, for future reference.

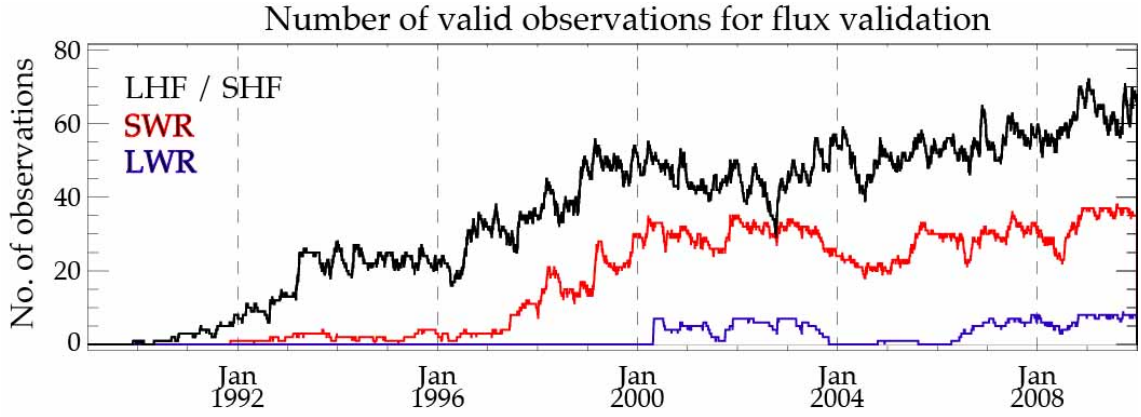

Figure 2. Number of high quality (quality flag 1 and 2) observations available for flux estimates from the TPR array. The black line shows the number of turbulent heat flux estimates, the red line the number of shortwave radiation estimates, and the blue line the number of longwave radiation estimates.

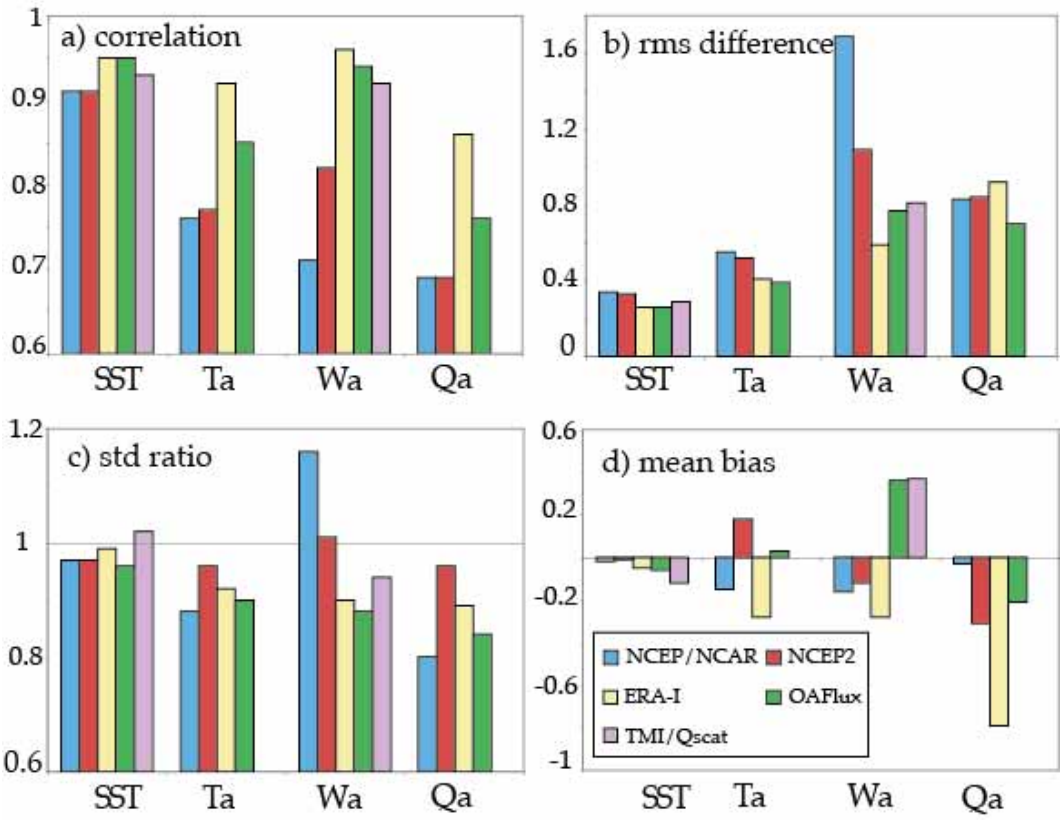

Figure 3: Evaluation statistics for Sea Surface Temperature (*SST*), Air Temperature (T_a), Specific Humidity (q_a) and Wind Speed (w_a) of the different products evaluated in this paper against tropical global mooring array data over the 2000-2009 period: (a) Correlation, (b) rms-difference, (c) ratio of standard deviation of the product to that of the mooring and (d) mean bias. All time series are subjected to 5 day smoothing before doing the statistics. The statistics are computed individually for each mooring, and we show the average of all individual moorings here. Various products are shown in different colors: blue for NCEP/NCAR, red for NCEP2, yellow for ERA-I, green for OAFlux and violet for TMI and Qscat.

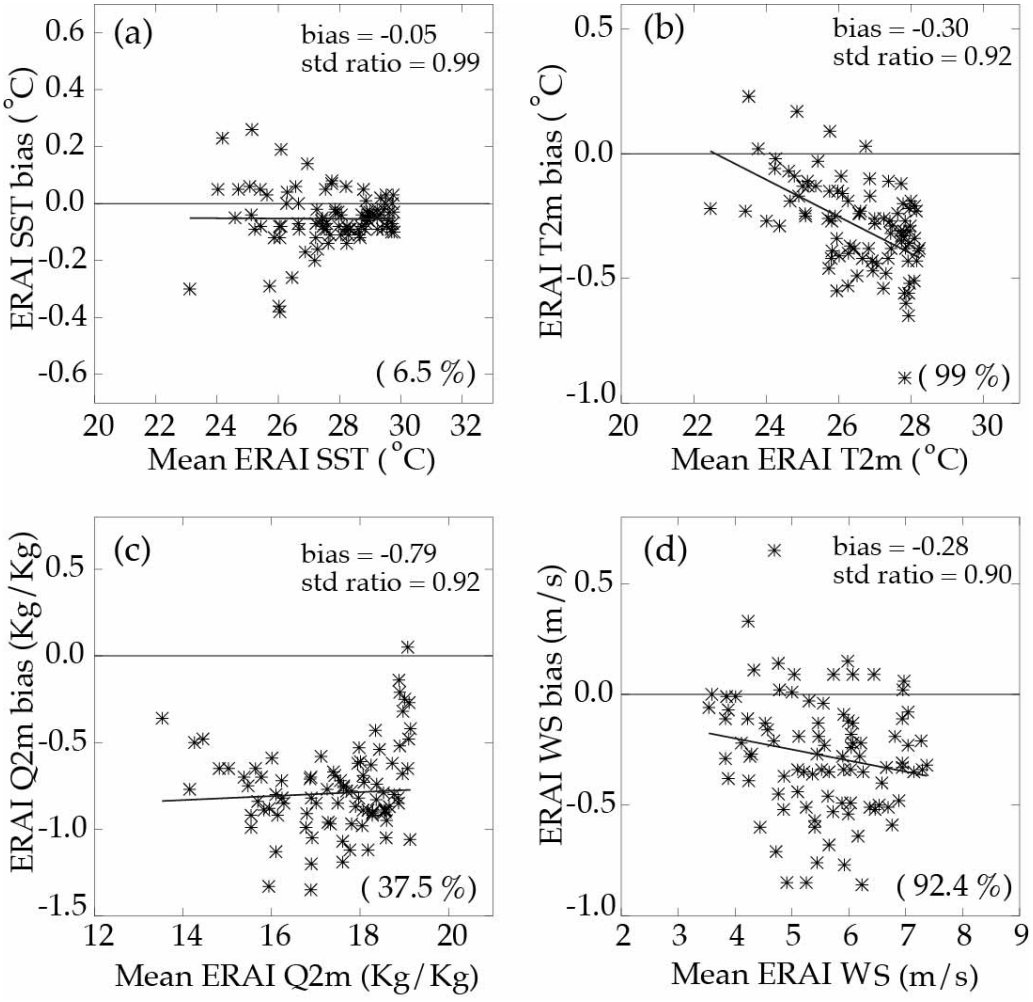

Figure 4: Scatter diagrams showing mean ERA-I values against ERA-I biases at TPR locations over the period 2000-2009 for (a) SST, (b) air temperature at 2m height, (c) specific humidity at 2m height and (d) wind speed at 10m heights. The slope of a linear fit and its confidence level are given on each graph.

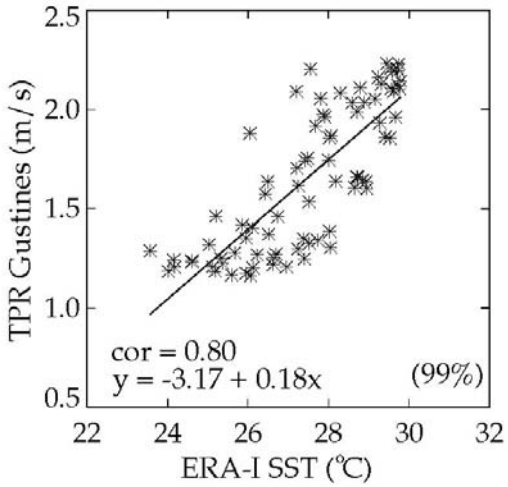

Figure 5: Linear fit between climatological TPR gustiness values from Cronin et al. (2006) against Climatological ERA-I SST. The linear fit is significant at 99% confidence level.

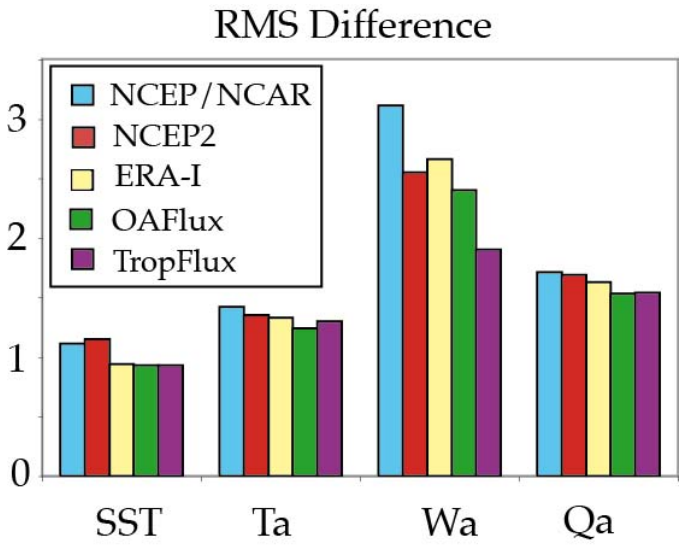

Figure 6: Bar diagrams-showing the root mean square difference of monthly ICOADS basic variables with other products over 1989-2009 periods. NCEP/NCAR is shown in blue, NCEP2 in red, ERA-I in yellow, OAFlux in green and TropFlux in purple (SST and Ta in °C, wind in ms^{-1}, humidity in kg/kg).

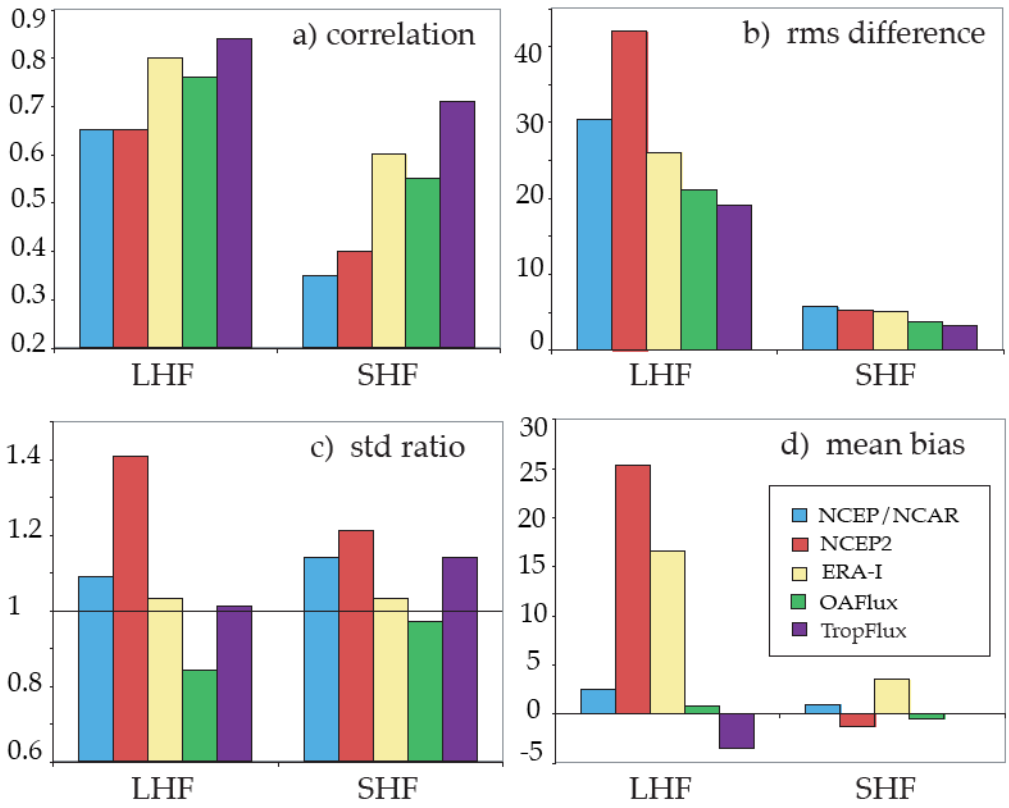

Figure 7: Bar diagrams-showing evaluations of 5-day average turbulent fluxes for the 2000-2009 period. NCEP/NCAR is shown in blue, NCEP2 in red, ERA-I in yellow, OAFlux in green and TropFlux in purple.

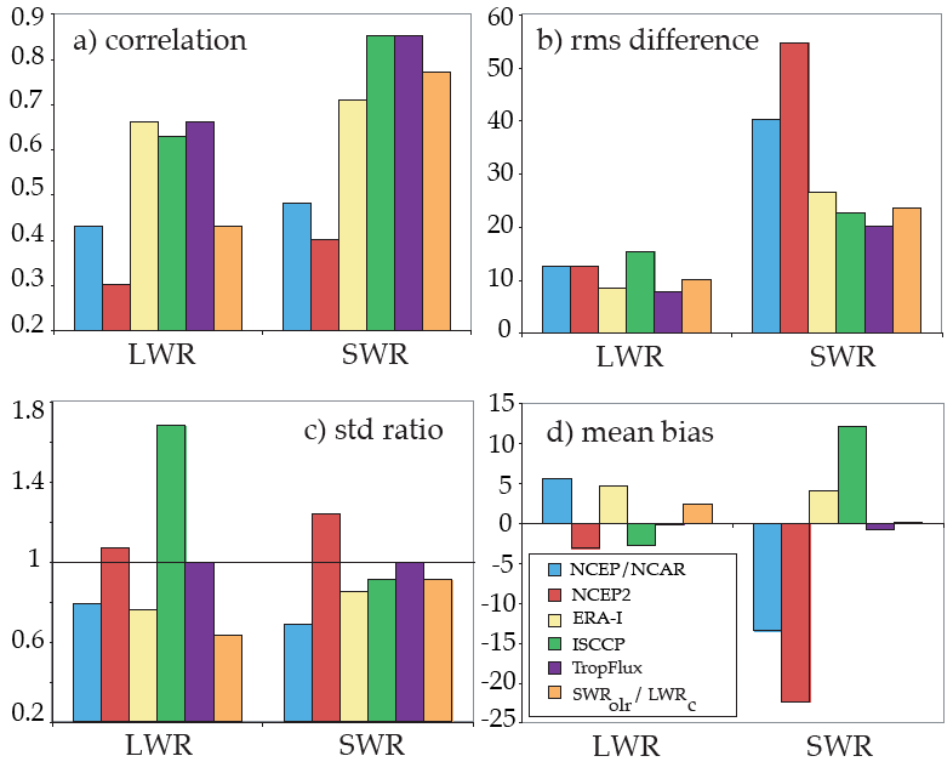

Figure 8: Bar diagrams-showing evaluation of 5-day average radiative fluxes for the 2000-2007 period. NCEP/NCAR is shown in blue, NCEP2 in red, ERA-I in yellow, ISCCP in green and TropFlux in purple. The orange bar shows the near-realtime reconstruction of SWR from OLR data and LWR from the Clark empirical formula.

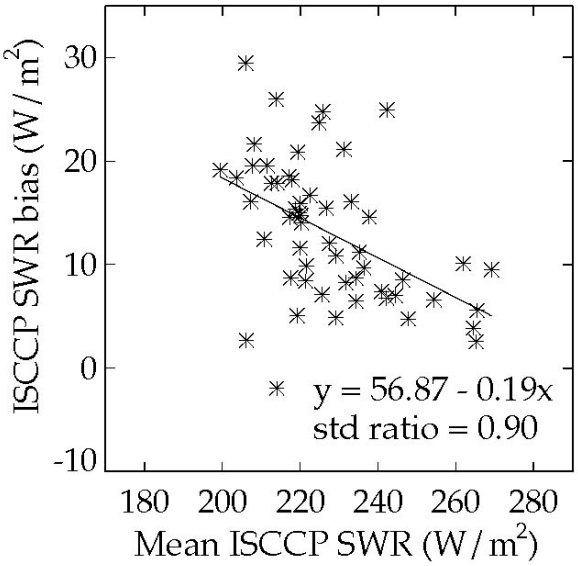

Figure 9: Scatter diagram of ISCCP SWR mean bias as a function of ISCCP long-term SWR. The linear fit is significant at 99% confidence level.

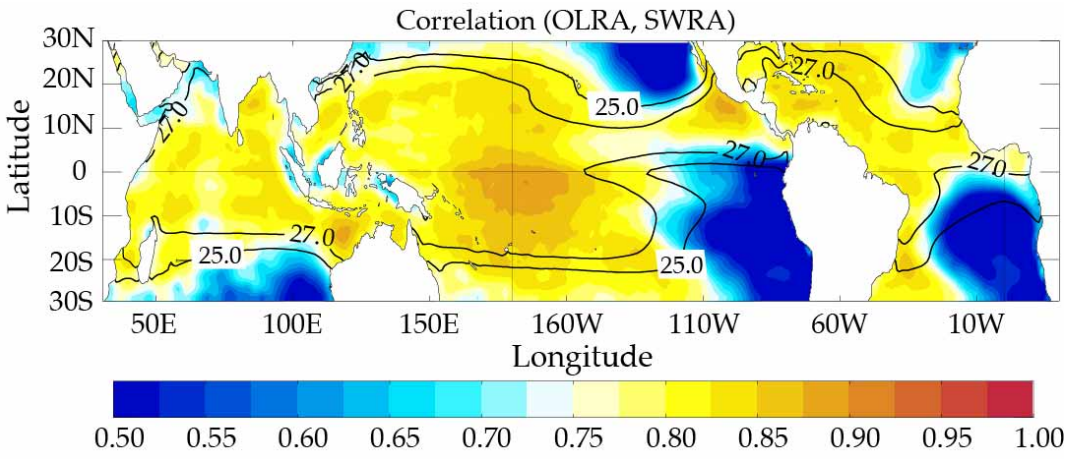

Figure 10: Correlation of OLR interannual anomalies with ISCCP SWR interannual anomalies. The contours show the climatological 25°C and 27°C isotherms.

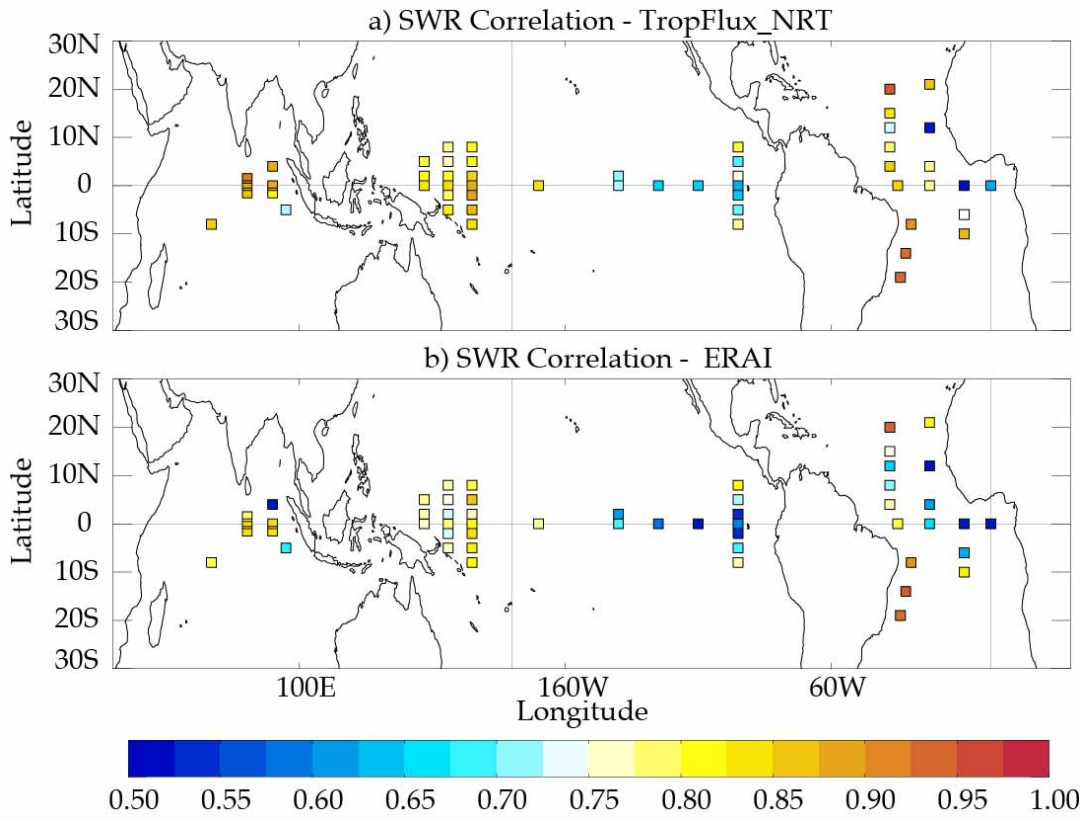

Figure 11: Correlation of shortwave radiation estimates with mooring measurements. The top panel shows correlation for the TropFlux NRT shortwave radiation while the bottom panel shows the same statistic for ERA-I shortwave radiation. The NCEP and NCEP2 re-analyses perform less well than ERA-I and are not shown. The statistics are based on 5-day smoothed data.

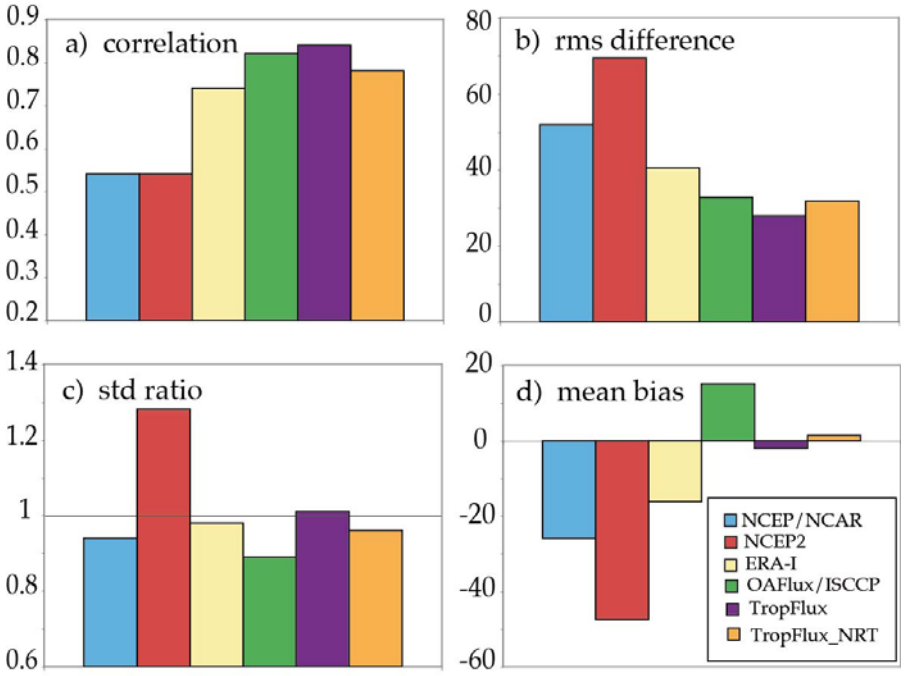

Figure 12: Bar diagrams showing evaluation of net flux over 2000-2007 periods. All time series are subjected to 5 day smoothing before doing the statistics. Here blue color denotes NCEP/NCAR, red denotes NCEP2, yellow denotes ERA-I, green denotes OAFlux/ISCCP, purple denotes TropFlux and orange denotes TropFlux_NRT.

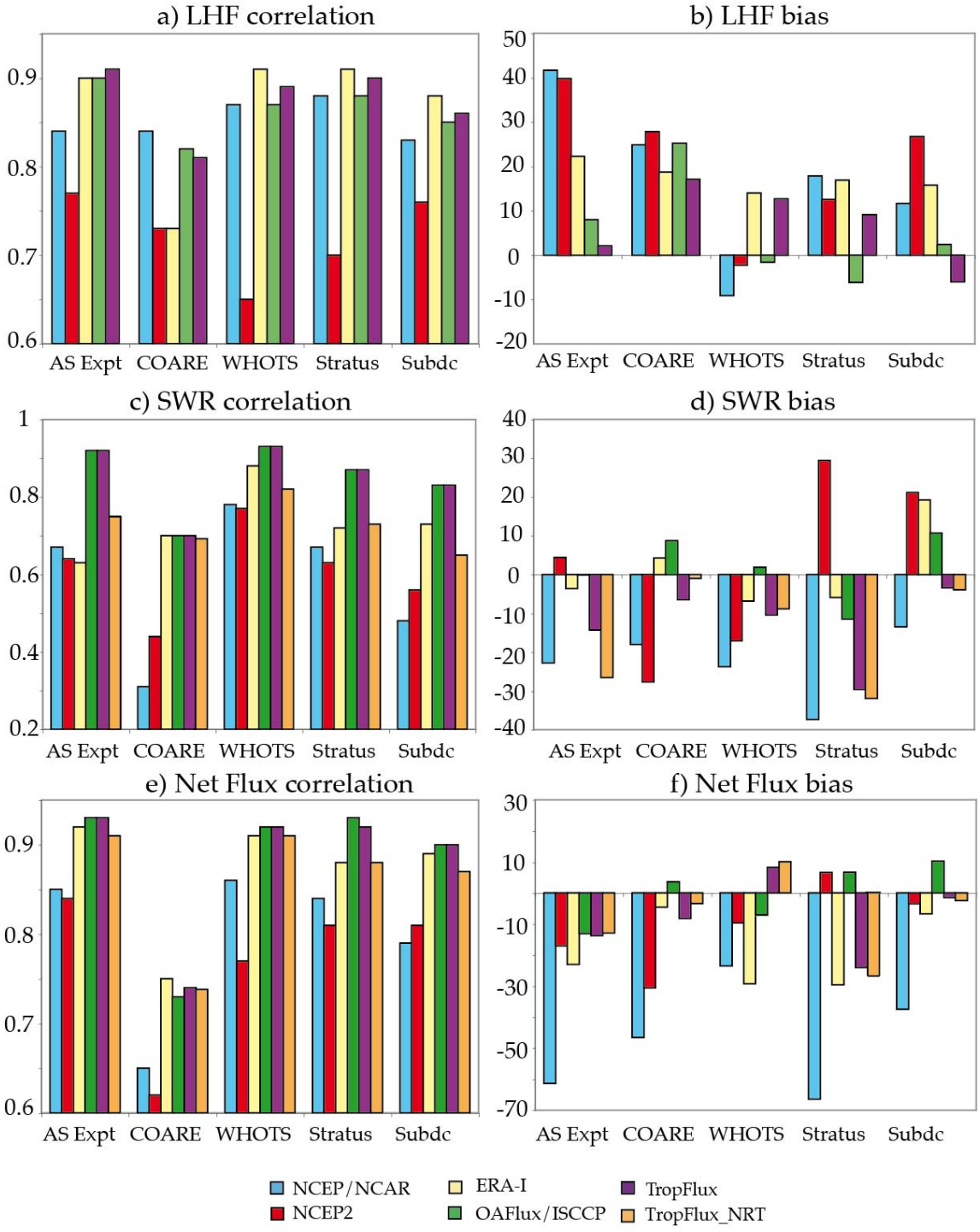

Figure 13: Bar diagrams showing validation of Latent Heat Flux (LHF), Shortwave Radiation (SWR) and net flux from different sources against that from five mooring locations. All the statistics shown are for daily values. Here blue color denotes NCEP/NCAR, red denotes NCEP2, yellow denotes ERA-I, green denotes OAFlux/ISCCP, purple denotes TropFlux and orange denotes TropFlux_NRT.

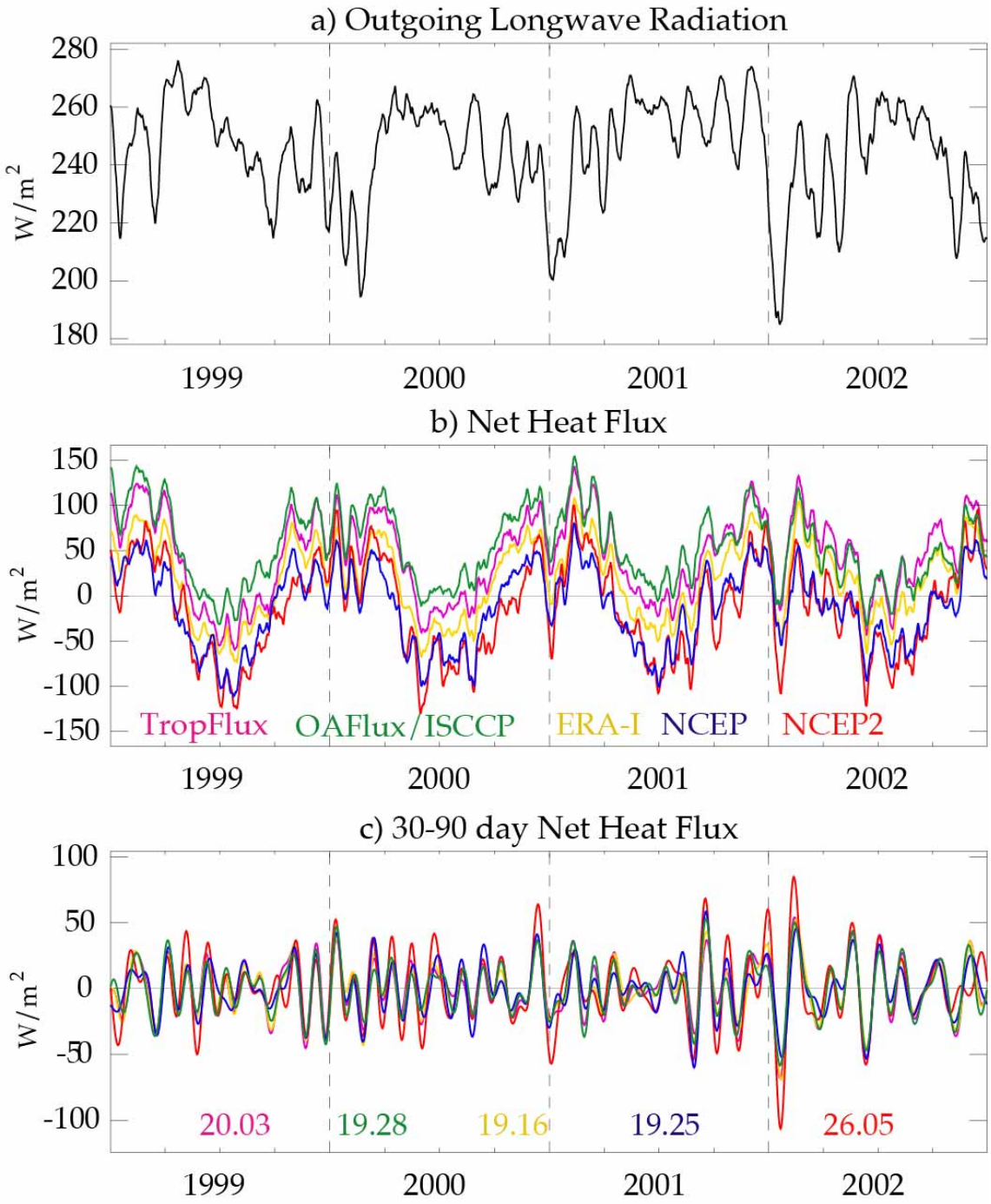

Figure 14: Time series of (a) Outgoing Longwave Radiation, (b) Net Heat Flux from different sources, and (c) 30-90 day filtered net heat fluxes, averaged over the thermocline ridge in the Indian Ocean (50°E-80°E and 12°S-5°S). The numbers shown in panel c are the standard deviation of the 30-90 day filtered net heat fluxes from different sources.

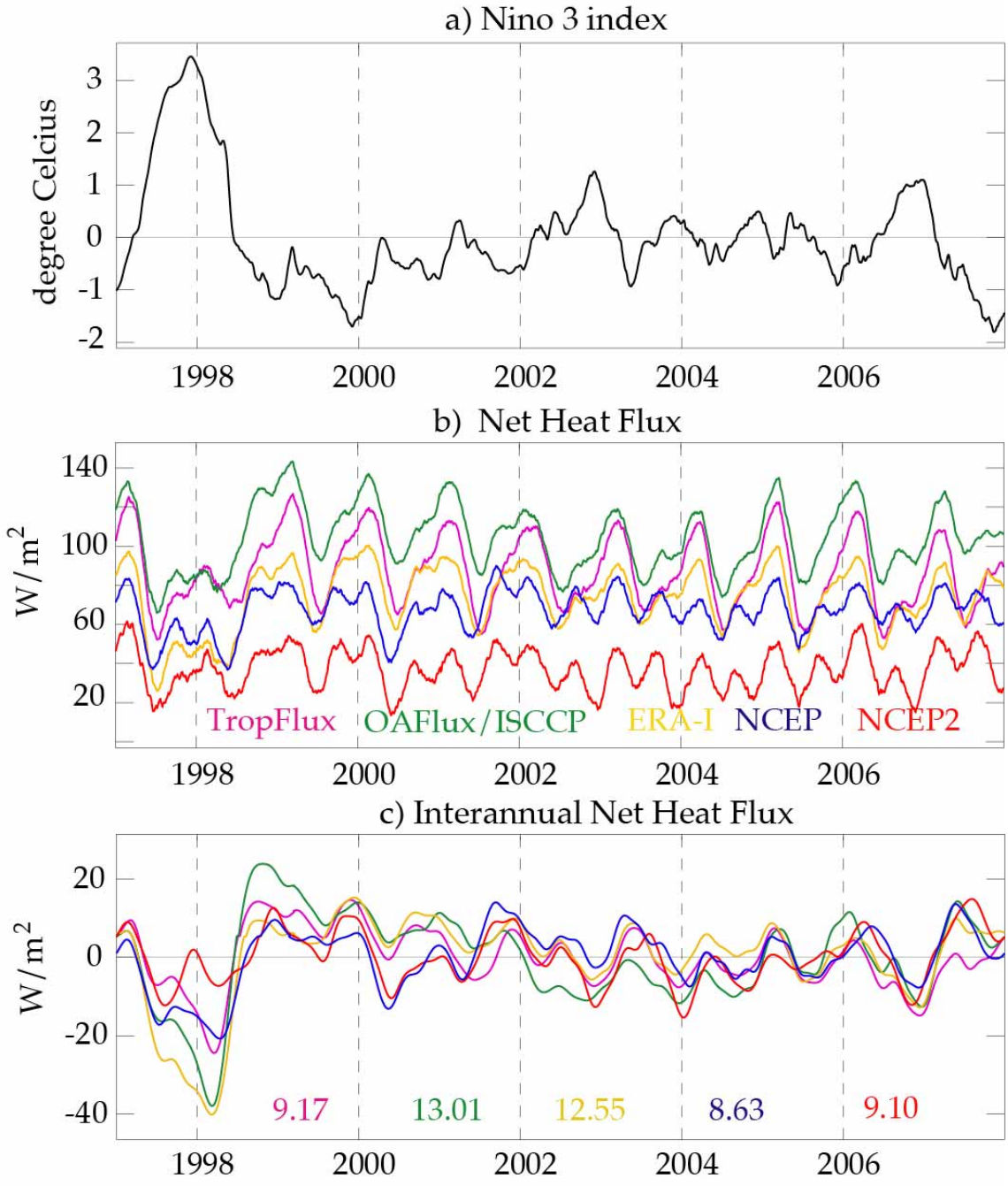

Figure 15: Time series of (a) Nino3 SST index, (b) Net Heat Flux from different sources, and (c) interannual anomalies of the net heat fluxes, averaged over the Nino 3 box (90°W-150°W and 5°S-5°N). The numbers shown in panel c are the standard deviation of the interannual net heat fluxes from different sources